

# Hydrography of the Red Sea and exchanges with the Indian Ocean in summer

Red Sea  
Bab al Mandab Strait  
Current  
Water masses  
Summer regime  
Mer Rouge  
Détroit de Bab el Mandeb  
Courant  
Masses d'eau  
Régime d'été

C. MAILLARD <sup>a</sup>, G. SOLIMAN <sup>b</sup>

<sup>a</sup> Institut Français de Recherche pour l'Exploitation de la Mer (IFREMER), Centre de Brest, B.P. 337, 29273 Brest Cedex, France.

<sup>b</sup> Institute of Oceanography and Fisheries, Kayet Bay, Alexandria, Egypt.

Received 21/3/85, in revised form 6/1/86, accepted 14/1/86,

## ABSTRACT

A cruise was carried out on board the R.V. "Marion Dufresne" in 1982 to follow the summer Red Sea regime and estimate the exchanges of water with the Indian Ocean. Two hydrographic surveys were made: one in early summer (June-July), the other in late summer (September-October). Between the two legs, a mooring of currentmeters was anchored in the Bab al Mandab Strait. Accordingly the three layers summer stratification was clearly observed in the Bab al Mandab Strait in June, and up to 18°N in October. The Indian Ocean inflow takes place at the intermediate level. Most of the return flow towards the Indian Ocean takes place in the surface layer due to the effect of the monsoon wind stress. The deep flow shrinks and sinks down to the narrow deep channel of the Bab al Mandab Strait. Correlatively the deep Red Sea warm water spreading in the Gulf of Aden is far less abundant at the end of summer than at the beginning of that season. In the Red Sea, some longitudinal variations have been observed in the deep water, showing mixing with the upper layers.

Simple empirical models are used to interpolate the depth of the interfaces in the Strait between the two surveys and, at a given time, to obtain the vertical profile of the velocity. Hence the time variations of the summer fluxes are estimated. The Indian Ocean intermediate inflow appears to be highest at the beginning of August with a value of  $0.36 \times 10^6 \text{ m}^3 \cdot \text{s}^{-1}$ , i.e. about 65% of the winter value given by Siedler (1968). As this inflow is mostly balanced with the surface current the magnitude of the deep Red Sea flow is then reduced to about 10% of the winter value.

*Oceanol. Acta*, 1986, 9, 3, 249-269.

## RÉSUMÉ

### Hydrologie de la Mer Rouge et de ses échanges avec l'Océan Indien en été

Une campagne a été réalisée en 1982 à bord du N.O. « Marion Dufresne » pour étudier le régime de mousson d'été en Mer Rouge et les échanges d'eau associés dans le détroit de Bab el Mandeb. Deux réseaux hydrologiques ont ainsi été exécutés l'un au début de l'été (juin-juillet), l'autre en fin de saison (septembre-octobre). Entre ces deux réseaux, un mouillage de courantométrie était mis en place. Les observations mettent clairement en évidence la structure estivale en trois couches, dans le détroit de Bab el Mandeb en juin, et jusqu'à 18°N à la fin de l'été. Le courant d'entrée issu de l'Océan Indien s'écoule dans la couche intermédiaire tandis que le flux profond d'eau chaude provenant de la Mer Rouge reste cantonné dans l'étroit chenal profond du détroit. Corrélativement, les eaux intermédiaires chaudes de la Mer Rouge dans le Golfe d'Aden occupent un volume nettement réduit et sont moins contrastées à la fin de l'été qu'en début de saison. Un trait marquant de l'eau profonde de la Mer Rouge a pu être mesuré : il s'agit d'une lente augmentation de la température profonde vers le sud traduisant le mélange avec les couches sus-jacentes.

Les profondeurs des interfaces ont été interpolées entre les deux legs de la campagne par un modèle empirique simple. Le profil vertical de vitesse dans le détroit de Bab el Mandeb a aussi été interpolé entre les points de mesure afin d'évaluer les débits d'eau

échangés entre la Mer Rouge et le Golfe d'Aden au cours de l'été. Le flux intermédiaire d'entrée a un débit maximal au début du mois d'août et se monte alors à  $0,36 \times 10^6 \text{ m}^3 \cdot \text{s}^{-1}$  soit 65% de la valeur hivernale de  $0,58 \times 10^6 \text{ m}^3 \cdot \text{s}^{-1}$  donnée par Siedler (1968). Ce flux est compensé en majeure partie par le courant de surface tandis que le courant profond d'eau chaude de la Mer Rouge ne représente plus qu'un flux d'environ 10% de sa valeur hivernale.

*Oceanol. Acta*, 1986, 9, 3, 249-269.

## GENERAL FEATURES OF THE RED SEA

Before presenting the 1982 data, the more salient features of the Red Sea will briefly be described. A detailed compilation of the knowledge of this region can be found in Morcos (1970). The Red Sea forms a semi-closed and very uneven basin connected with the Indian Ocean and the Gulf of Aden by the narrow Strait of Bab al Mandab. The surrounding lands are mountainous deserts and the climate depends on the monsoon regime. Upon those peculiar conditions, the Red Sea appears as a concentration basin with a deep salty water mass formation and with large seasonal variations in the upper layers.

## Bathymetry

The Red Sea forms a long and narrow trench, roughly NNW-SSE oriented, about 1930 km long and 270 km wide between 12°N and 28°N. North of 28°N the sea is bounded by the shallow Gulf of Suez to the west and the deep Gulf of Aqaba on the eastern side (Fig. 1). The continental shelf (less than 50 m depth) is widely extended in the southern half of the Red Sea. The central trough more than 1000 m deep is found north of 16°N; its width is about 50 km and the deepest parts reach 2700 m. The sills region which separates the Red Sea from the Indian Ocean stretches over a rather long distance. The shallower sill lies in the north of the Hanish archipelago at 13°44'N and its depth is 137 m (Werner, Lange, 1975). The Strait of Bab al Mandab is the narrowest area where the main channel, west of the Perim Island (12°34'N) is about 300 m deep.

## Evaporation, thermohaline forces and sea surface level

Evaporation is very high with an estimated value of 2 m/year which results in a loss of  $0,03 \times 10^6 \text{ m}^3 \cdot \text{s}^{-1}$  over the whole area of the Red Sea ( $450 \times 10^3 \text{ km}^2$ ). The seasonal variations of the evaporation are a much debated question and do not exceed the accuracy of the estimation. Precipitation is negligible. The most important effect of evaporation is to increase the salinity, and consequently the density, of the surface water. The resulting pressure gradient creates an upper inflow of water from the Indian Ocean towards the Red Sea and an outflow of deep and dense Red Sea water in the opposite direction. Both of these flows drive a volume of water far higher than the volume of evaporated water. The average transported volumes of inflowing and outflowing water have been estimated to be  $0,33 \times 10^6 \text{ m}^3 \cdot \text{s}^{-1}$  by Siedler (1969) from the conservation of salt condition and the average value of evaporation.

From long time series (23 years) of tide gauges at Suez, Perim and Port Sudan, Patzert (1972) has shown that the sea level differences between the points of observation remain within 0.3 m. Moreover he established that the effects of the pressure gradients due to these slopes are smaller than the wind stress and that the surface circulation is primarily wind driven.

## Winds and surface drift current

The predominant winds blow towards the SSE everywhere except during the winter season in the southern half of the sea where they are directed towards the

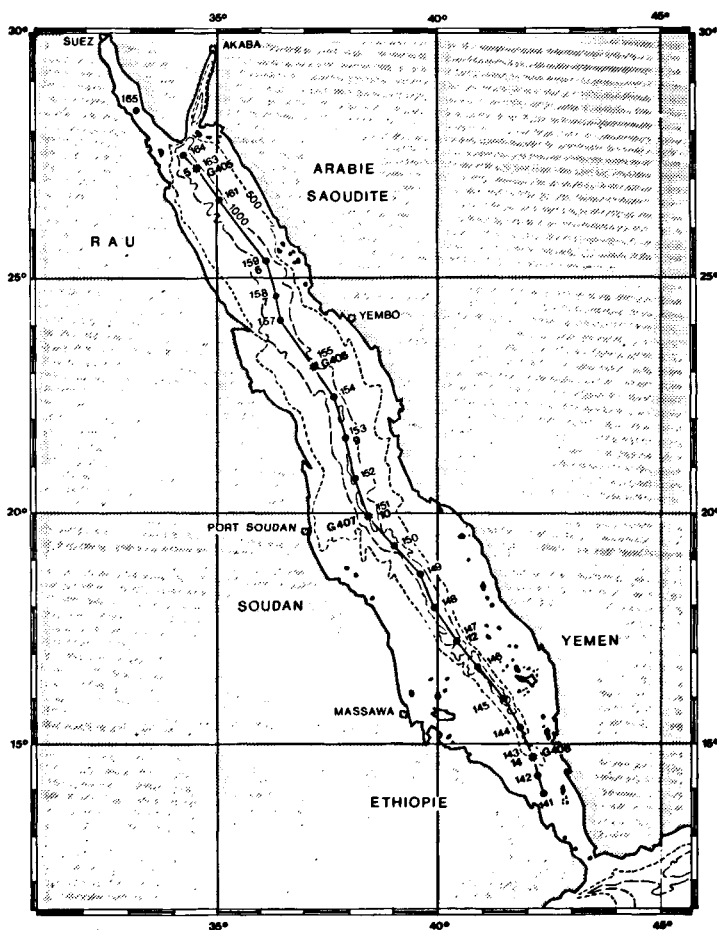


Figure 1

CTD stations of the "Marion Dufresne" cruise (1982) in the Red Sea.

First leg: 26 to 30 June, stations 5 to 14.

Second leg: 3 to 8 October, stations 141 to 165.

Stations CTD de la campagne « Marion Dufresne » (1982) en Mer Rouge.

Premier leg : 26 au 30 juin, stations 5 à 14.

Deuxième leg : 3 au 8 octobre, stations 141 à 165.

NNW. Thus in winter the wind stress intensifies the upper inflow of Indian Ocean water. Conversely, from June to mid-September the wind stress acts against this inflow.

The surface current and its seasonal variations have been studied from ship drift observations (KNMI Atlas, 1949; Patzert, 1972). They show that to the south of 19°N, the monthly average surface current is very similar to the wind stress distribution. During the summer months (June to September), the surface current is a shallow drift layer which flows towards the SSE, whereas the Indian Ocean inflow and the deep Red Sea water sink at a deeper level. The surface flow reaches its maximum intensity in August with an estimated flux of  $0.21 \times 10^6 \text{ m}^3 \cdot \text{s}^{-1}$ . The available direct current observations made in the winter season indicate a surface flow of  $0.58 \times 10^6 \text{ m}^3 \cdot \text{s}^{-1}$  towards the NNW (Vercelli, 1927; Siedler, 1968).

North of 19°N, the surface flow towards the SSE appears over a longer period of time in the year (June to October) than in the southern Red Sea. In addition, eddies and meanders seem to occur frequently, which makes it difficult to estimate the mean current from the ship drifts along a limited number of shipping routes.

#### Hydrography of the Red Sea during the winter season

In winter, two main water masses are present in the Red Sea. The surface water originating from the Indian Ocean, about 80 m deep, is warm and fresh, but undergoes strong cooling and concentration between the southern and the northern boundaries of the sea. On the contrary, the deep water is very homogeneous below the sill depth, with  $T \approx 21.7^\circ\text{C}$ ,  $S = 40.57$ . The overflow of this water, in the Bab al Mandab Strait region, does not keep those characteristics, as the mixing with the surface layer is here very active. The deep flux has about the same magnitude as the surface inflow.

The sinking of the surface water in the vicinity of the northern boundary is assumed to be mostly a winter process. The main convective flow is created by the mixing of the very dense Gulf of Suez water (which is far colder and saltier than the Red Sea deep water) with the north Red Sea subsurface water (Maillard, 1974). More recent observations (Hassan, Soliman, in preparation) show that an important contribution to the deep water formation also comes from the shallow coastal waters of the northern Red Sea outside the Gulf of Suez. The existence of a large permanent cyclonic gyre in this region (Bibik, 1968; Maillard, 1971; Morcos, Soliman, 1971) can also strengthen the vertical motions and the deep water formation.

#### Summer regime

In summer the wind stress and the thermohaline forces have opposite effects, and a decrease of the exchanges with the Indian Ocean is to be expected. Very few data are available for that season. Three water masses are

present. The surface wind driven current flows towards the SSE. The Indian Ocean inflow takes place below, and the Red Sea deep water outflow is very reduced. According to Neuman and Mc Gill (1961), this three-layer scheme just begins in July in the southern part of the Bab al Mandab Strait but is not yet found further north. The northernmost limit of the cold subsurface inflow of Indian Ocean water has been observed at 18°20'N in October (Jones, Browning, 1971; Robinson, 1973).

From the average historical data (Siedler, 1968), the Red Sea deep water appears colder by  $0.1^\circ\text{C}$  and saltier by 0.05 in summer than in winter. This is a high variability for a deep water mass but it has been confirmed by some recent observations (Baudner *et al.*, 1984).

#### Theoretical studies

Phillips (1966) computed the longitudinal thermohaline circulation from the density distribution, and an estimation of the dissipation corresponding to the data of Neuman and Mc Gill in early summer with negligible winds. Siedler (1968) gave a relation between the current interface and the density interface. Patzert (1972) estimated the monthly average longitudinal flow in each degree of latitude taking into account the monthly mean values of wind, the corrected sea level and the density gradient. Wyrki (1974) studied the deep water dynamics resulting from the vertical convection and the diffusion of several conservative and non conservative parameters. Neglecting the horizontal advection in the deep layer, he gave an estimation of  $0.2 \times 10^{-6} \text{ m} \cdot \text{s}^{-1}$  for the vertical ascending velocity and of 72 years for the residence time of the deep water. Van Akken and Otto (1974) formulated the critical conditions for transforming the two-layer into the three-layer regime (and inversely), as a function of the pressure gradient, the surface stress and the bottom depth. Soliman (1979) constructed numerical models with one and two layers similar to the Patzert's model, but with a finer grid including the transverse variations.

All those models have been performed to study the effect of a few schematized parameters on some specific characteristics of the Red Sea dynamics. The results do not fit the data very well and are rather disappointing. The reason is certainly that the conditions (bathymetry, winds...) are very variable and complicated, and that the set of available data is too loose to give a good physical description of the phenomena.

#### DATA COLLECTED DURING THE "MARION DUFRESNE" CRUISE OF 1982

The purpose of the "Marion Dufresne" cruise during summer 1982 was then to enlarge the available data set concerning this lesser known season, and to estimate the water exchanges between the Red Sea and the Indian Ocean with hydrographic sections, direct current measurements and chemical sampling. The results of the physical observations are presented here.

The experiment was carried out in two legs, one during the early summer (26 June to 4 July), the other at the end of this season (9 September to 8 October). The same hydrographic survey was to be done at each leg, and two currentmeter moorings were laid out in the Bab al Mandab Strait for the whole season. The positions of the CTD stations (numbers above 100 for the second leg) and the currentmeter moorings are shown (Fig. 1 and Fig. 2).

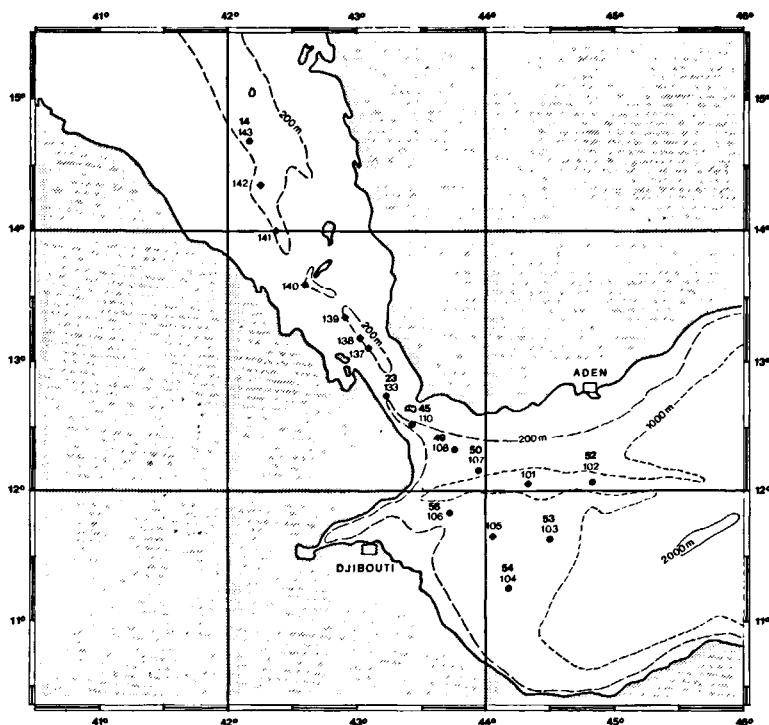


Figure 2a  
 CTDO stations along the main channel of the Bab al Mandab straits region and the Gulf of Aden.  
 First leg: 30 June to 3 July, stations 21 to 56.  
 Second leg: 26 September to 3 October, stations 101 to 142.  
 Stations CTDO le long de l'axe central du détroit de Bab el Mandeb et dans le Golfe d'Aden.  
 Premier leg : 30 juin au 3 juillet, stations 21 à 56.  
 Deuxième leg : 26 septembre au 3 octobre, stations 101 à 142.

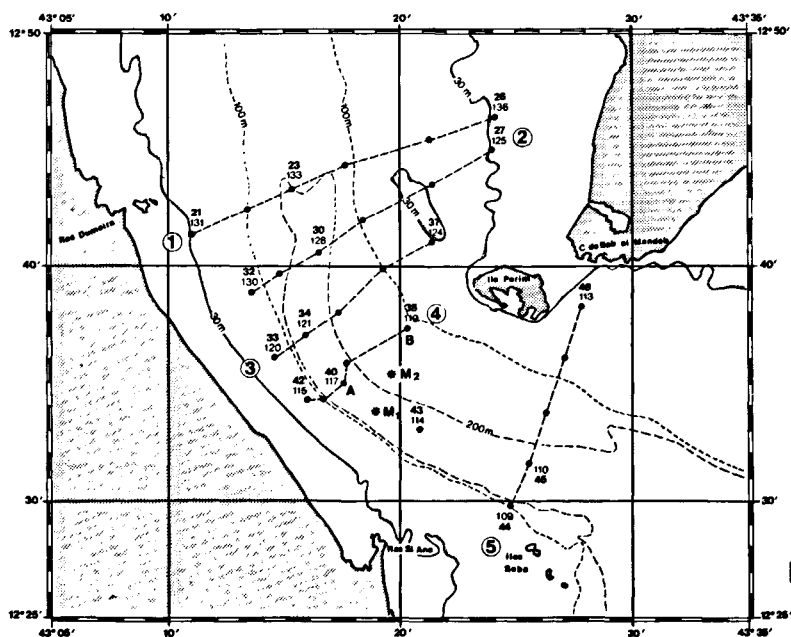


Figure 2b  
 CTDO stations at five vertical cross-sections (1 to 5) in the Bab al Mandab strait and a "tide section" AB.  $M_1$  and  $M_2$  are the positions of the currentmeter moorings.  
 Stations CTDO aux sections transversales 1 à 5 dans le détroit de Bab el Mandeb et section marée AB. Les points  $M_1$  et  $M_2$  représentent les points de mouillage de courantométrie.

During the June leg, 41 CTD stations were made: 7 stations along the longitudinal central fault of the Red Sea, 28 stations along five cross-sections in the Bab al Mandab Strait and 6 stations in the Gulf of Aden. Due to some trouble with the CTD board receiver, only the temperature/pressure profiles were then recorded. The moorings  $M_1$  and  $M_2$  were set in the

deep part of the narrowest section of the Strait (Fig. 2b).

During the September leg, the moorings were released but only the mooring  $M_2$  at  $12^{\circ}35'N$ ,  $43^{\circ}20'E$  by 189 m depth on the eastern slope of the deep channel was recovered. The hydrographic survey was made afterwards at the same sites as during the June leg with

a few extra stations: 8 stations in the Gulf of Aden, 28 stations in the Bab al Mandab Strait, 24 stations along the Red Sea section and one station in the Gulf of Suez. In the northern half of the Gulf of Suez, the conductivity of the sea water overstepped the available scale of the CTD sensor. The complete description of the physical data collected during the cruise can be found in Maillard and Soliman (1985). The most significant features will be presented here.

The studied characteristics will generally be abbreviated taking T for temperature (the only parameter recorded during the first leg),  $\theta$  for potential temperature, S for salinity and  $O_2$  for oxygen concentration.  $\sigma_\theta$  is the Knudsen's parameter (=potential density — 1000, in MKS units) and is used for potential density. The salinity units are p.s.u.

### HYDROGRAPHY OF THE DEEP RED SEA IN SUMMER 1982

The upper layers of the Red Sea present a high time and space variability. On the contrary, below the sill depth (137 m), the temperature and salinity distributions are very homogeneous. This situation is typical of concentration basins. Consequently the longitudinal vertical section had to be presented in two parts: a) the upper 200 dbar; b) the deeper than 200 dbar water.

In the Red Sea, the temperature distribution during the June section (Fig. 3) still shows the winter two-layered pattern, as was already observed by Neuman and Mc Gill in June 1958. In October the three-layer summer regime is settled in the southern Red Sea. The Indian Ocean inflow takes place between 30 and about 80 dbar; it presents marked minima of temperature and salinity with  $\theta \leq 20^\circ\text{C}$ ,  $S \leq 37$ . This vein can be traced as far as  $18^\circ\text{N}$ , but north of  $16^\circ 40'\text{N}$  its temperature and salinity increase steeply. A large eddy or meander centered near  $17^\circ 20'\text{N}$  is detected at the head of this

subsurface flow; the vertical perturbations on the isolines  $\theta=23^\circ\text{C}$  (Fig. 4a) and  $S=38.5$  (Fig. 5a) indicate that the diameter is about 250 km. The core of the Indian Ocean inflow has a relatively stable density  $\sigma_\theta=25.5$ . Along the whole section the isopycnals show a general tendency to rise northwards in the upper layers (Fig. 6a). So the  $\sigma_\theta=25.5$  isopycnal reaches the free surface near  $23^\circ 30'\text{N}$ . At that location the isolines present, below the thermocline in October (50 dbar) a 100 dbar deepening on about 200 km. This marks the presence of another eddy but unfortunately no measure was made here in June and it is not possible to know if that feature was present. In May 1983 a very similar pattern has been found a little more south near  $22^\circ\text{N}$  (Quadfasel, pers. comm.) and can very likely be attributed to the same eddy.

Below 200 dbar the water is very homogeneous. The largest part of the deep water has the characteristics  $\theta=21.60^\circ\text{C}$ ,  $S=40.60$ ,  $\sigma_\theta=28.60$  and the variations remain respectively within  $0.5^\circ\text{C}$ , 0.20, 0.4. The variations are mainly due to the vertical gradient, but some horizontal trend has also been detected in temperature and density. At a given level the temperature increases from the north of the sea to the south, and the density decreases. Thus at 1000 dbar the characteristics increase regularly from  $\theta=21.43^\circ\text{C}$ ,  $\sigma_\theta=28.64$  in the northern Red Sea (station 163) to  $\theta=21.63^\circ\text{C}$ ,  $\sigma_\theta=28.58$  near  $15^\circ\text{N}$  (station 144, Fig. 4b, 6b). Although small, those differences are significant and show the exchanges by mixing, convection and diffusion with the overlying surface water during the southeastward transport of the deep layer. At the same level and below, the horizontal variations of the salinity do not exceed the accuracy of the measure  $\Delta S=0.01$ . During the 1963 winter (Maillard, 1974) the deep temperature was far more homogeneous: the potential temperature below 800 dbar was  $\theta=21.54 \pm 0.03^\circ\text{C}$ . So the longitudinal temperature gradient of the deep Red Sea water could be only a summer process.

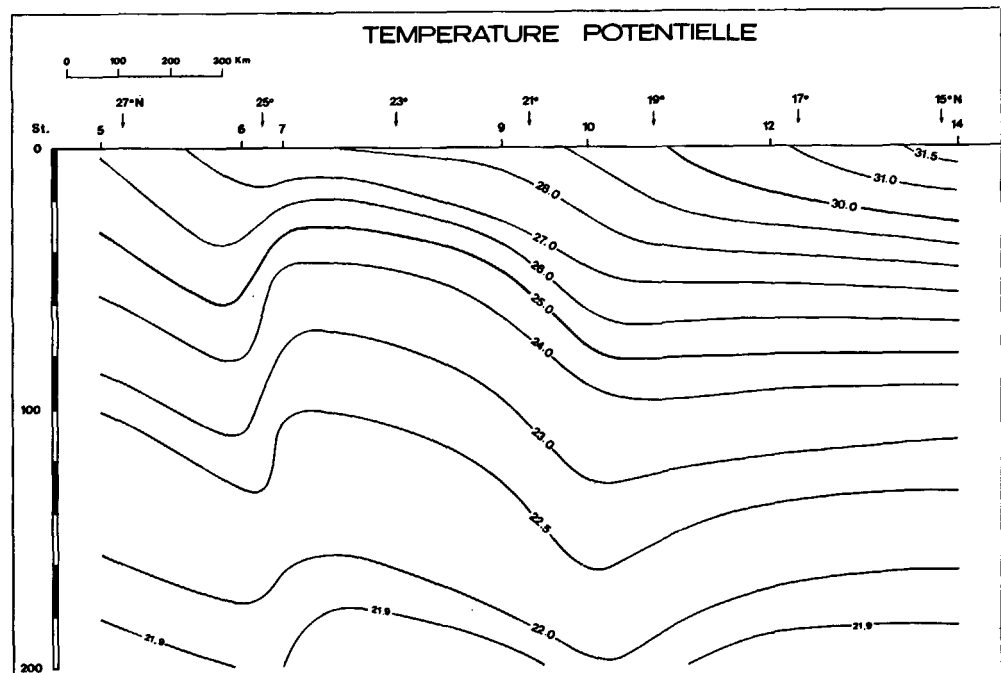
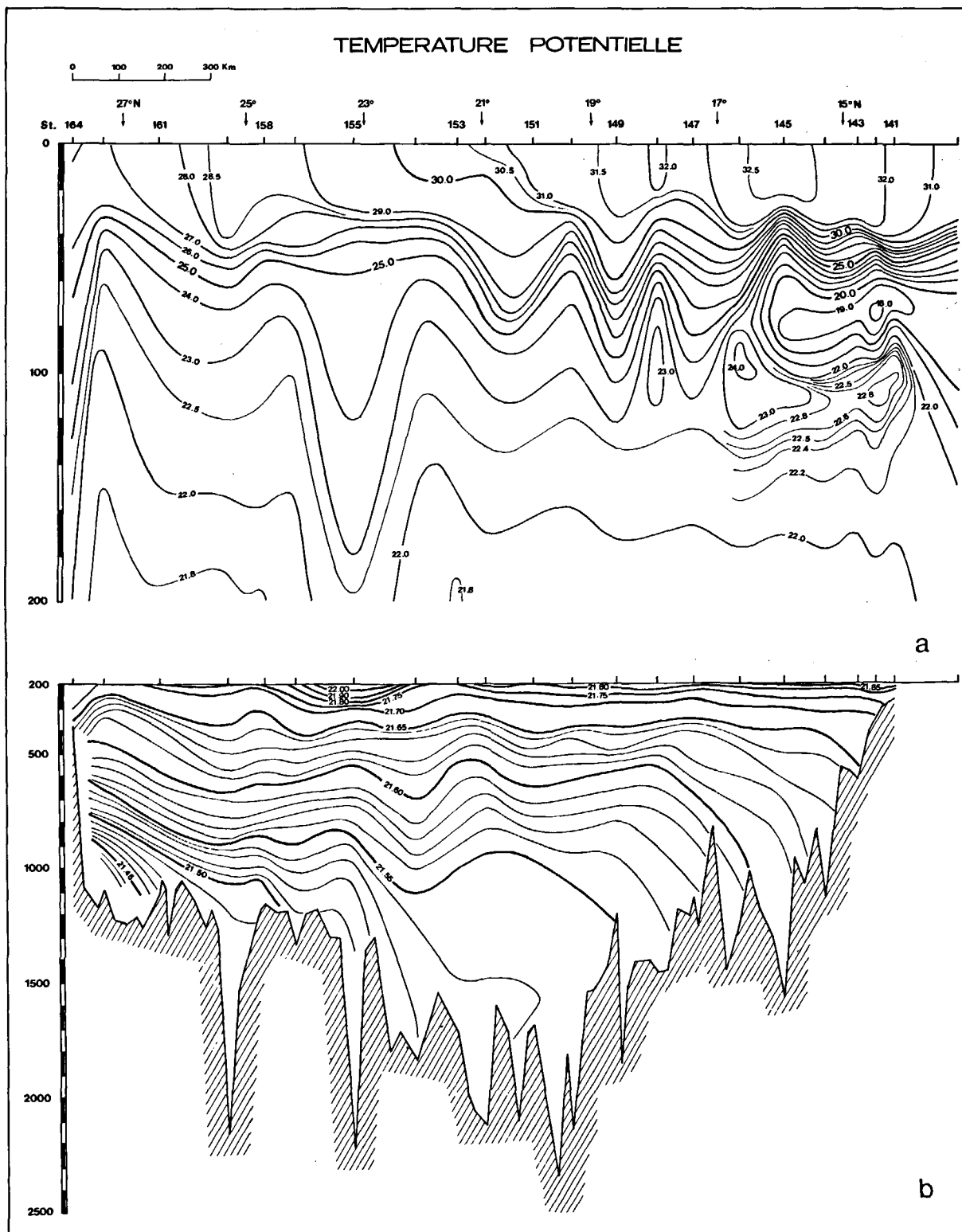


Figure 3  
Upper temperature distribution in the Red Sea in June.  
Température dans les couches supérieures en juin en Mer Rouge.



**Figure 4**  
*Vertical potential temperature distribution in the Red Sea in October:*  
 a) above 200 dbar;  
 b) below 200 dbar.

Section verticale de température potentielle en octobre en Mer Rouge :  
 a) au-dessus de 200 dbar ;  
 b) au-dessous de 200 dbar.

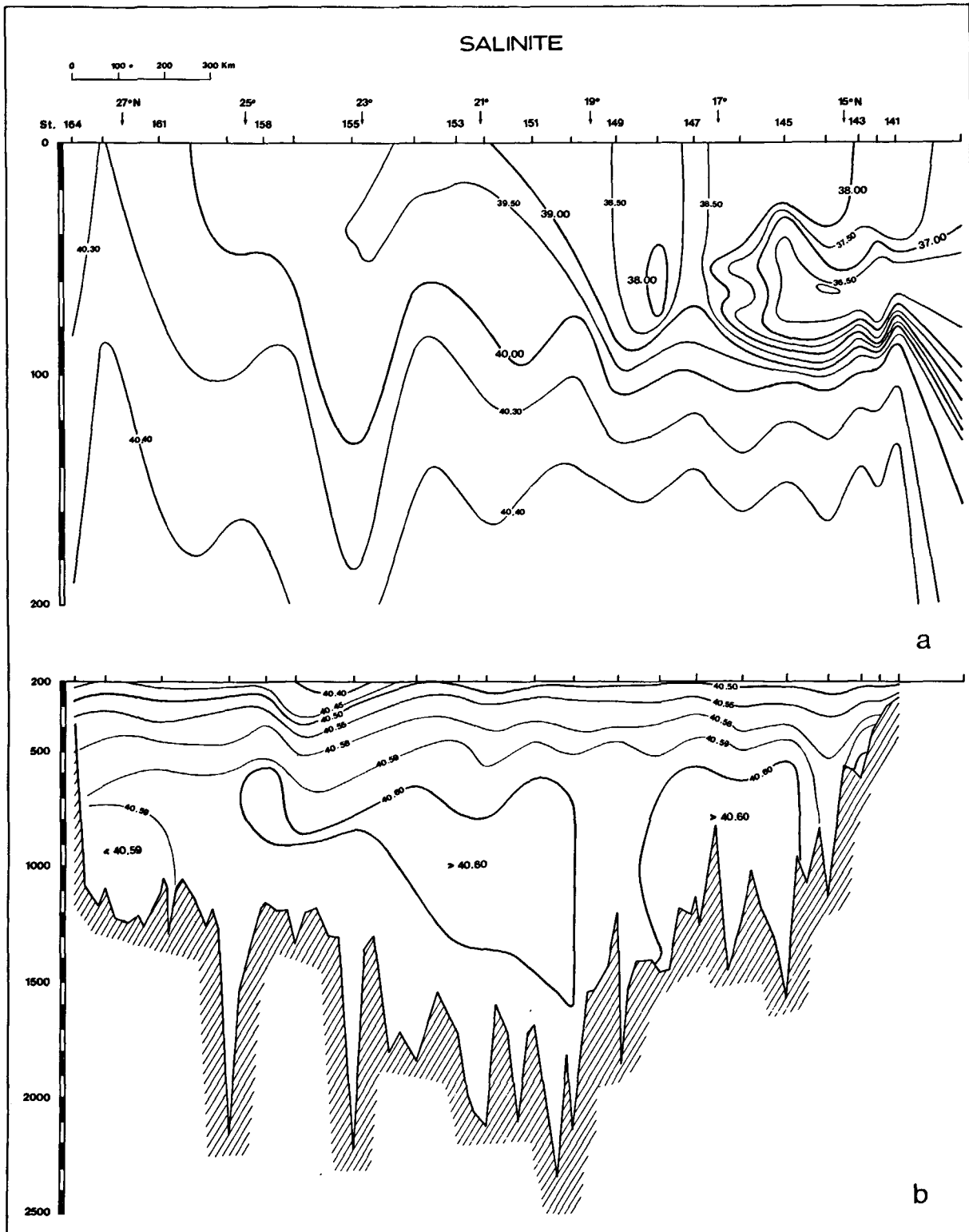
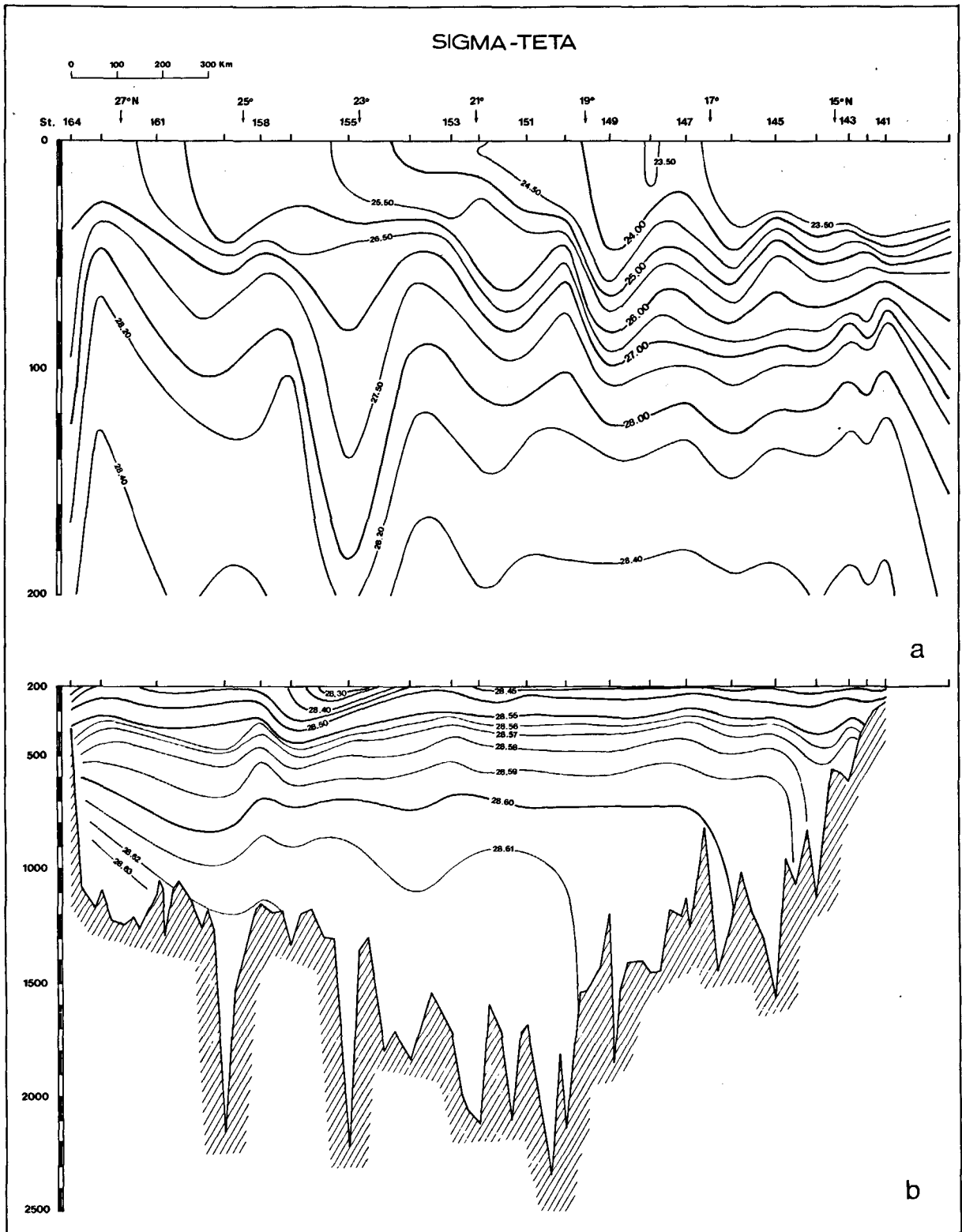


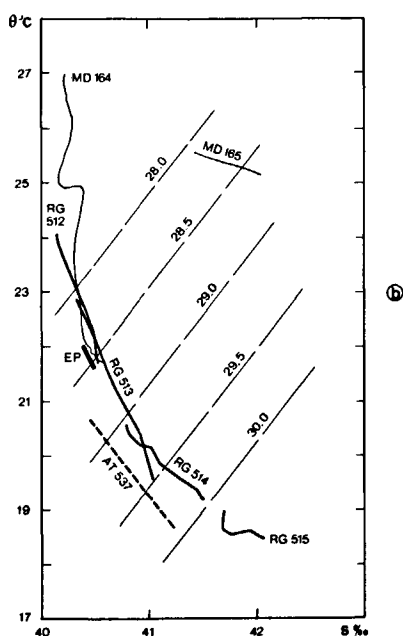
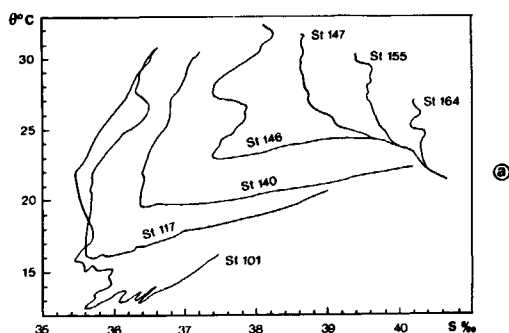
Figure 5  
 Vertical salinity distribution in the Red Sea in October:  
 a) above 200 dbar;  
 b) below 200 dbar.  
 Section verticale de salinité en octobre en Mer Rouge :  
 a) au-dessus de 200 dbar;  
 b) au-dessous de 200 dbar.



**Figure 6**  
 Vertical potential density (sigma-theta) distribution in the Red Sea in October:  
 a) above 200 dbar;  
 b) below 200 dbar.  
 Section verticale de densité (sigma-theta) en octobre en Mer Rouge :  
 a) au-dessus de 200 dbar;  
 b) au-dessous de 200 dbar.

**Figure 7**  
 Evolution of the  $\theta$ -S diagrams:  
 a) in the deep Red Sea and the near Gulf of Aden;  
 b) in the Gulf of Suez and the northern Red Sea.  
 Évolution des diagrammes  $\theta$ -S :  
 a) dans la Mer Rouge profonde et le proche Golfe d'Aden;  
 b) au nord de la Mer Rouge et dans le Golfe de Suez.

The October  $\theta$ -S diagrams (Fig. 7a) show mostly the evolution of the upper layers from the Gulf of Aden (station 101) to the northern Red Sea (station 164). In the southern region, the water is strongly stratified with three layers on the vertical. In the northern region, the water column is nearly homogeneous and the length of the  $\theta$ -S curve is very short. The deep Red Sea water which fills most of the basin is represented by a very small segment on this diagram. The question whether any deep water is formed during the summer season can be investigated by considering the  $\theta$ -S diagrams of the northern Red Sea and Gulf of Suez waters in October (Fig. 7b, Marion Dufresne, station 164 and 165) and in February (Robert Giraud 1963, stations 512 to 515; Atlantis 1965, station 537). The late summer values of salinity are practically the same as the winter values at the same geographical site and reach  $S=42$  in the Gulf of Suez. The temperatures are about  $6.5^\circ\text{C}$  higher in late summer than in winter, and therefore are not able to form any deep water by mixing with the Red Sea subsurface water present above the slope. Yet it is very likely that some sinking of water occurs due to the high densities found in the northern Red Sea, but only intermediate waters are formed. This would explain the small irregularities on the  $\theta$ -S curve at the shelf station 164. The formation of intermediate water of high salinity in the northern Red Sea can be a step towards the winter deep water formation.



## THE SILL AND BAB AL MANDAB STRAIT REGION

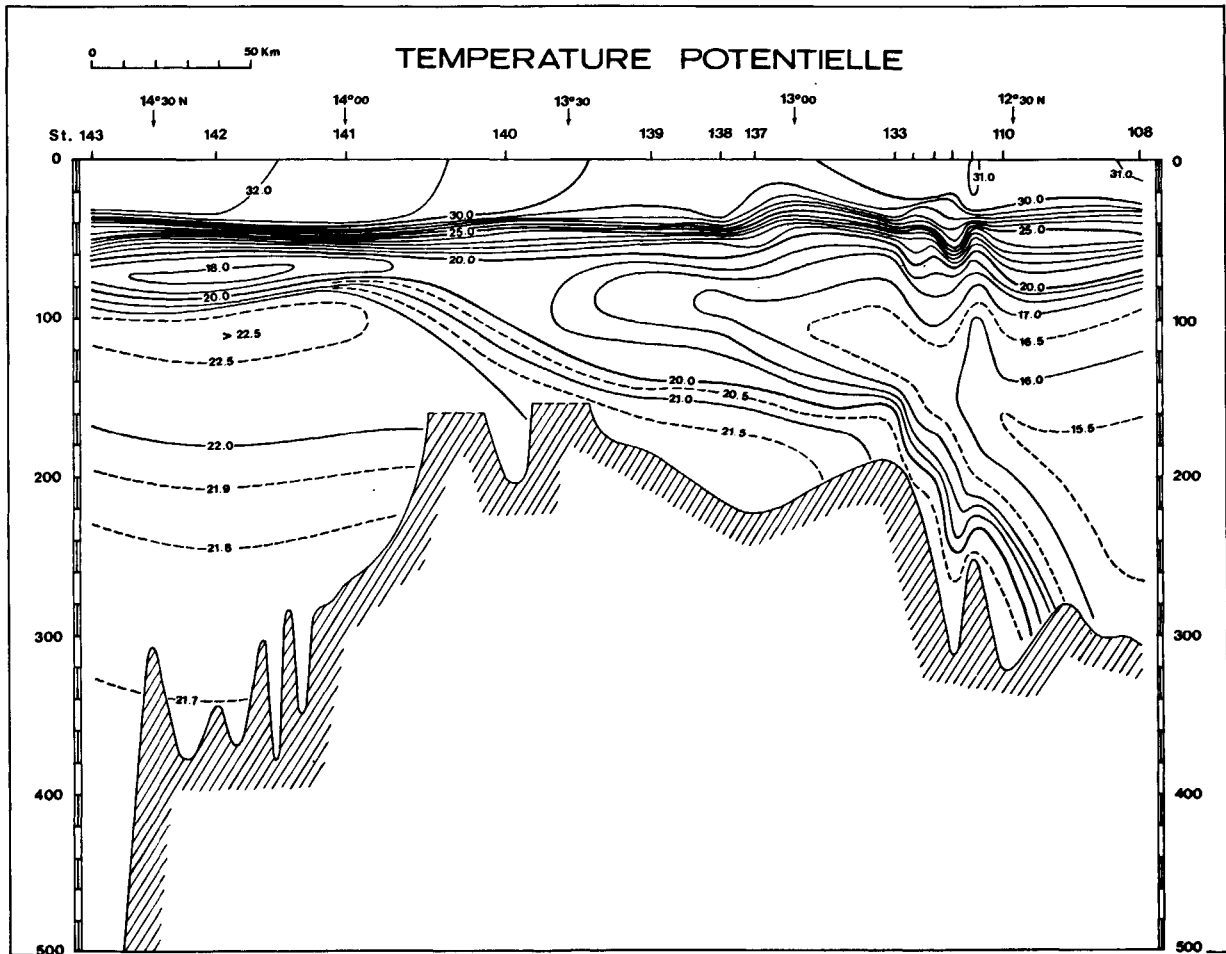
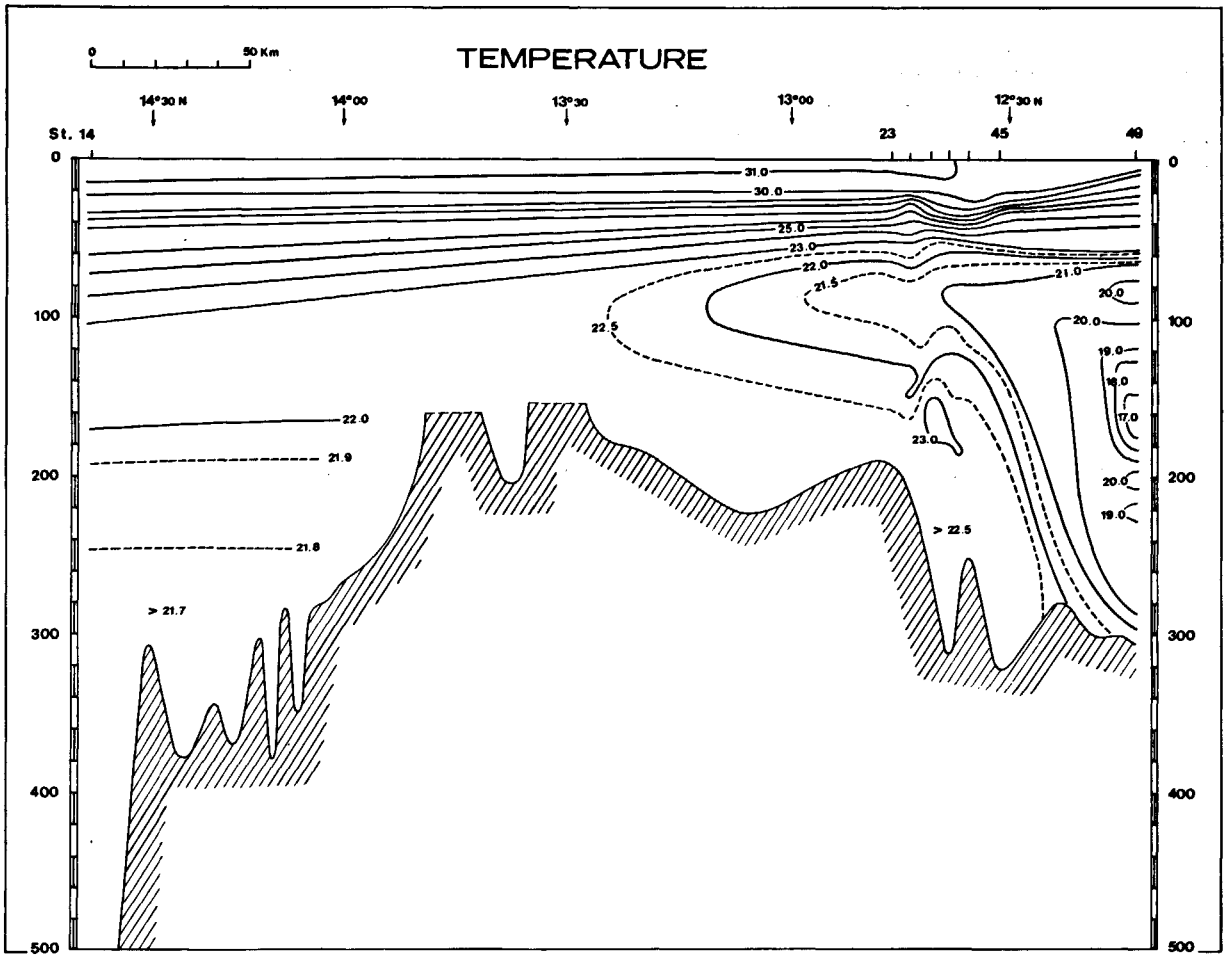
Over the Bab al Mandab Strait region, the three-layer stratification takes place from June (Fig. 8), but has not yet reached the shallowest point of the sill at  $13^\circ44'N$ . In June-July, the core of the Indian Ocean intermediate flow is found around 90 dbar in the Strait and has a temperature between  $20.5$  and  $21.5^\circ\text{C}$ . In October, the core of this inflow is found at a deeper level, near 150 dbar (Fig. 9) and has a lower temperature:  $\theta \leq 16^\circ\text{C}$  in the Bab al Mandab Strait. Over the Hanish sill (station 140), the thickness of the intermediate flow shrinks to about half the value it had in the Strait (station 110-133), which is certainly due to the shoaling and the widening of the channel in the sill region.

The deepest layer is filled with Red Sea water. Just north of the sill, a temperature and oxygen (Fig. 11) maximum appears between 90 and 170 dbar with  $22.0 \leq \theta \leq 22.9^\circ\text{C}$  and  $2.0 \leq O_2 \leq 3.0$  ml/l. This maximum indicates the level where the deep Red Sea water of the Strait is drawn. No corresponding maximum appears on the salinity distribution (Fig. 10), probably because the salinity gradient between the Indian Ocean water and the Red Sea water is too steep. The characteristics of the deep Red Sea water change very much along the sill region and the Strait of Bab al Mandab in October. The volume of the Red Sea water is reduced, the layer is thinner than 40 dbar in the narrow central channel and the mixing with the overlying cold and fresh water is intensive. The density of this Red Sea water (Fig. 12) is higher by 1. than the density at the same level in the Gulf of Aden. So the deep isopycnals sink southwards and the deep Red Sea water is supposed to move along them.

If the intermediate and deep layers appear very variable in time and space, the surface layer seems relatively stable. In June as in October, the surface temperature lies around  $30.5^\circ\text{C}$  everywhere in the Strait region. The other characteristics appear also rather homogeneous except the oxygen content which takes maximum surface values  $O_2 \approx 6$  ml/l in the Strait (Fig. 11).

The cross-sections made in the Bab al Mandab Strait (Fig. 13-14) give at the same time the transverse variations in the water masses and a better estimation of their volume. The Indian Ocean intermediate water is colder and thicker against the eastern side of the channel, which results from the effect of the Coriolis force. In June-July, the core of this layer lies between 80-120 dbar and has  $T \leq 21^\circ\text{C}$ . At the same time a second core appears in the southernmost sections 4 and 5; this layer is deeper (150-170 dbar) and colder with  $T \leq 20^\circ\text{C}$ . In October no double core has been observed.

The effect of the Coriolis force in the deep Red Sea water was only detectable in June. Then a core of maximum temperature, with  $T \geq 22^\circ\text{C}$  near 160 dbar on section 1, and  $T \geq 23^\circ\text{C}$  near 200 dbar on section 5, appears against the western side of the Strait. The southward increase of temperature in the deep Red Sea



◀ Figure 8  
*June-July longitudinal section of temperature in the sill and Bab al Mandab Strait region.*  
 Section longitudinale de température dans la région des seuils et du détroit de Bab el Mandeb en juin-juillet.

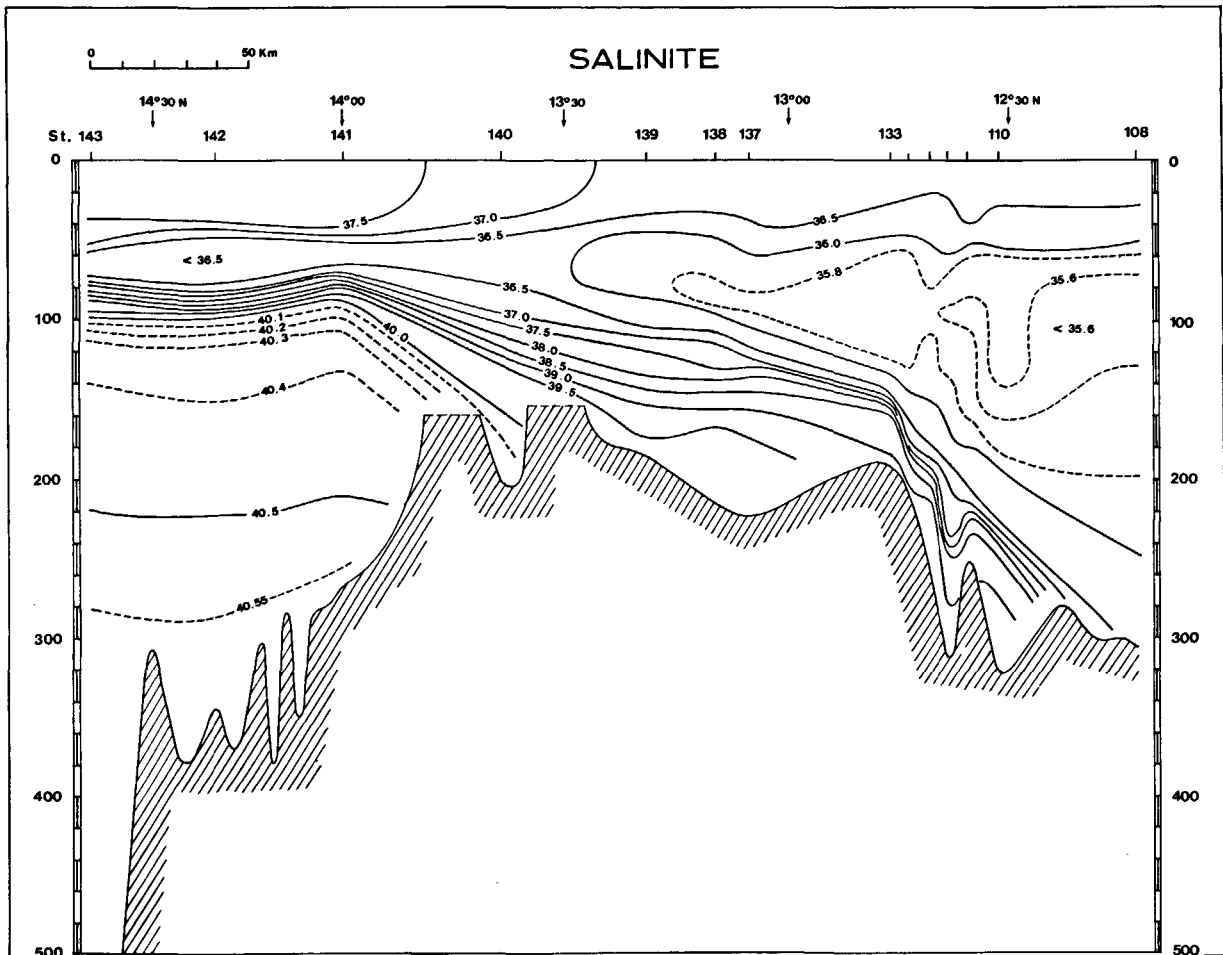


Figure 10  
*September-October longitudinal section of salinity in the sill and Bab al Mandab Strait region.*  
 Section longitudinale de salinité dans la région des seuils et du détroit de Bab el Mandeb en septembre-octobre.

cannot be due to the mixing with the cold overlying layer. In fact the time of the observations is the transition period between the two regimes: the flow of Red Sea water is slowing down and interests only the lowest (and coldest) part of the initial layer. In October the deep Red Sea is colder  $\theta \leq 19^\circ\text{C}$  and is confined to the very narrow central trough.

Across section 4 near Perim Island, two stations A and B (see the positions on Fig. 2b) have been investigated during 27 hours on 1 and 2 October, to determine the tidal interface variability. Eleven CTD stations were made within a circle of 0.5 nautical mile radius around each site. In the resulting potential temperature time series (Fig. 17a and b) the semi-diurnal tidal signal is visually apparent. The quantitative relationship between the depth of the isotherms and the tide prediction available for the same period of time south of the Strait has not been established. It was too difficult to

take into account the variations of amplitude and phase along the vertical upon this rather short time series. A striking point is that the depth of the isotherms is far shallower during this tide section than it was two days before at the same section 4 (Fig. 16), meaning a very fast change too at this time of the year.

#### SPREADING OF THE RED SEA WATER IN THE NEAR GULF OF ADEN

The Gulf of Aden hydrography appears very complicated. The surface layer is shallow, warm, salty and oxygenated:  $\theta \approx 30^\circ\text{C}$ ,  $S \approx 36.6$ ,  $\text{O}_2 \approx 4.5$  ml/l and relatively homogeneous. Below, several contrasted layers associated with  $\theta$ ,  $S$ ,  $\text{O}_2$  maxima and outflowing from the Red Sea, overlap other layers associated with minima of the same parameters and originating in the Indian

◀ Figure 9  
*September-October longitudinal section of potential temperature in the sill and Bab al Mandab Strait region.*  
 Section longitudinale de température potentielle dans la région des seuils et du détroit de Bab el Mandeb en septembre-octobre.

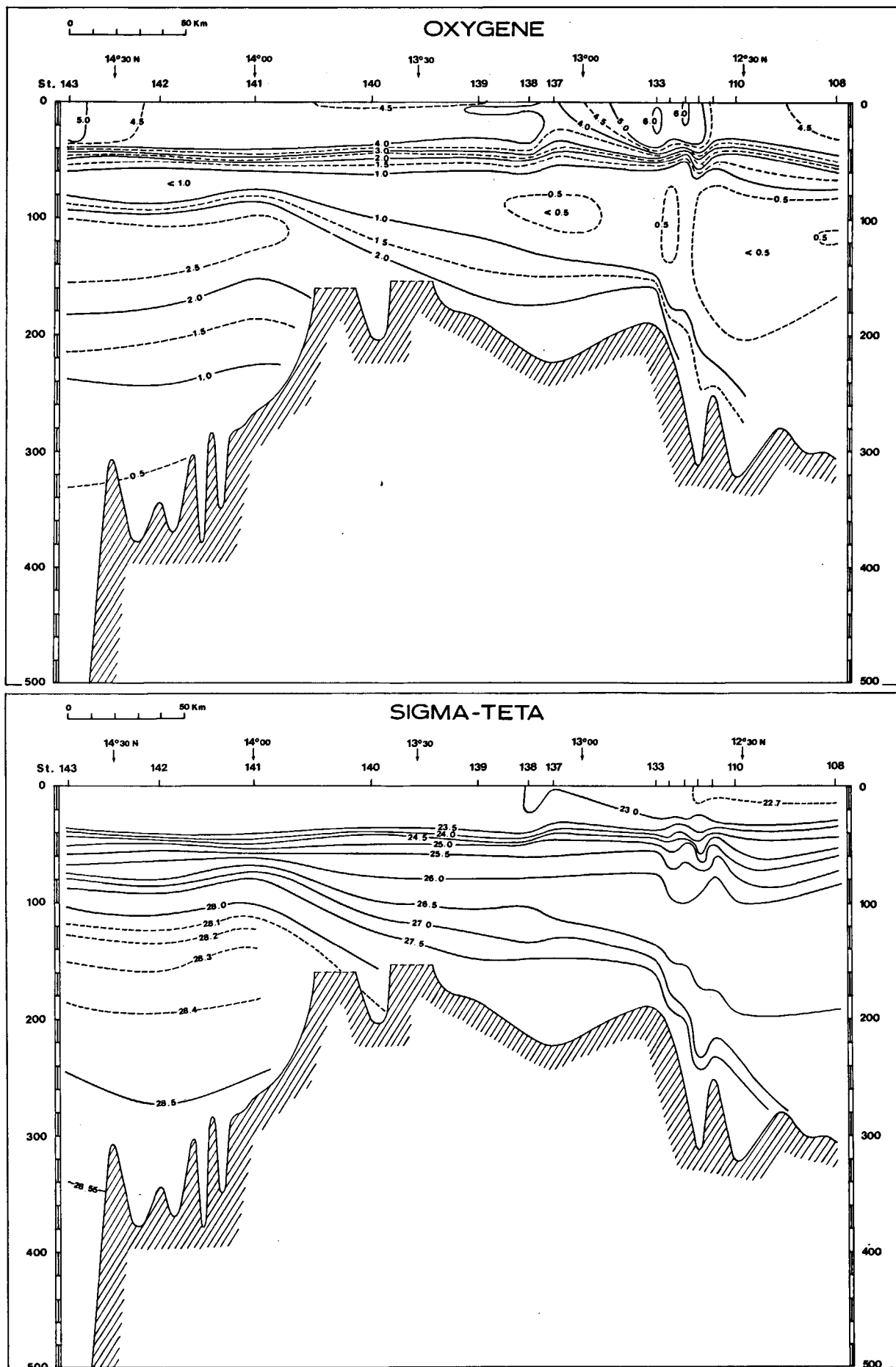


Figure 12  
 September-October longitudinal section of density in the sill and Bab al Mandab Strait region.  
 Section longitudinale de densité dans la région des seuils et du détroit de Bab el Mandeb en septembre-octobre.

Figure 11

September-October longitudinal section of oxygen in the sill and Bab al Mandab Strait region.

Section longitudinale d'oxygène dans la région des seuils et du détroit de Bab el Mandeb en septembre-octobre.

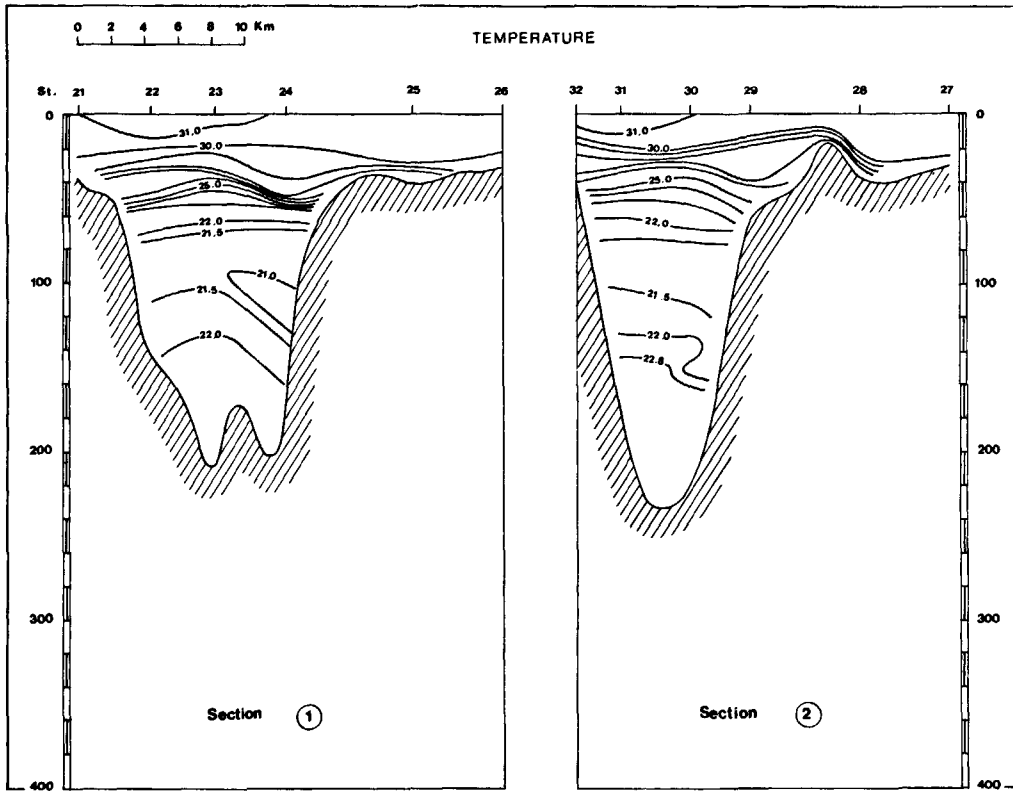


Figure 13

Vertical distribution of temperature in June along the transversal sections 1 and 2 of the Bab al Mandab Strait.

Répartition verticale de température le long des sections transversales 1 et 2 du détroit de Bab el Mandeb en juin.

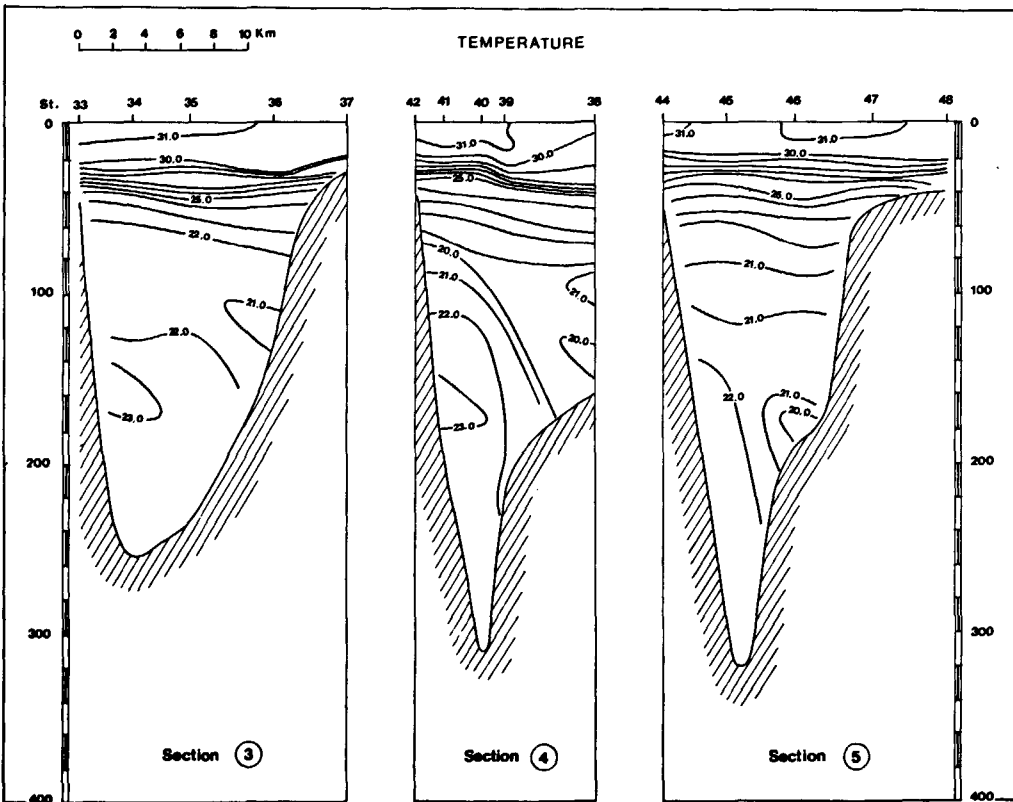


Figure 14

Vertical distribution of temperature in June along the transversal sections 2, 4 and 5.

Répartition verticale de température le long des sections transversales 3 à 5 du détroit de Bab el Mandeb en juin.

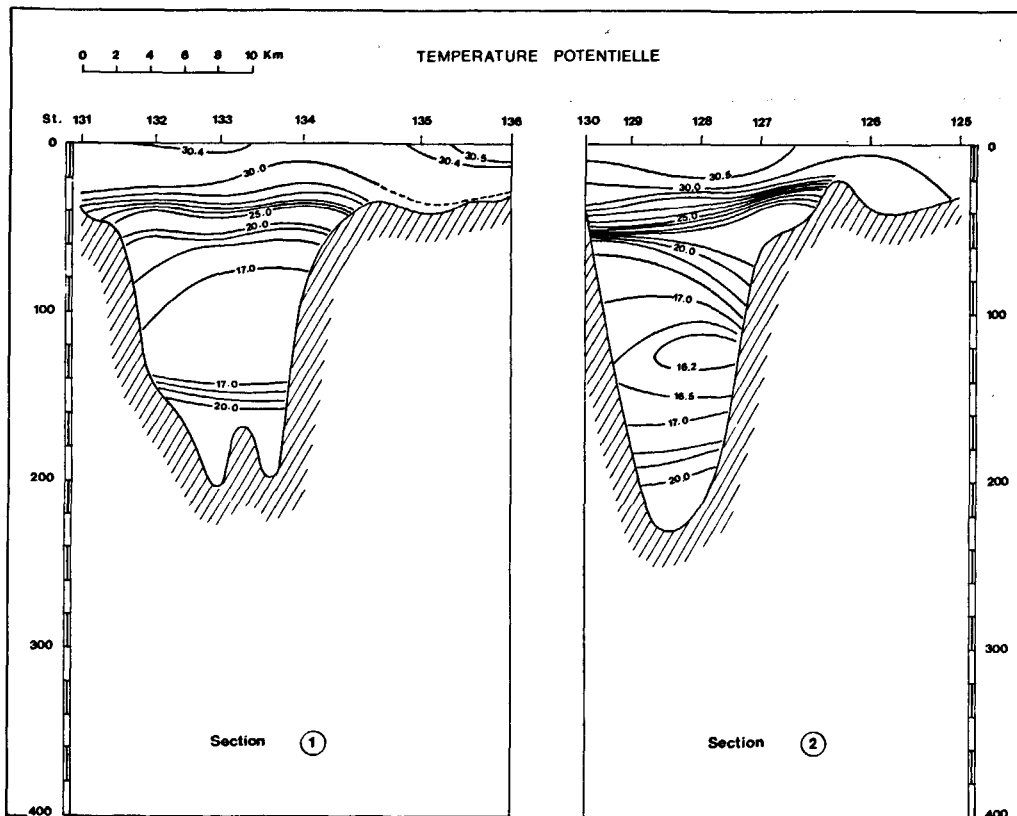


Figure 15  
 Vertical distribution of potential temperature in September along the transversal sections 1 and 2.  
 Répartition verticale de température potentielle le long des sections transversales 1 et 2 du détroit de Bab el Mandeb en septembre.

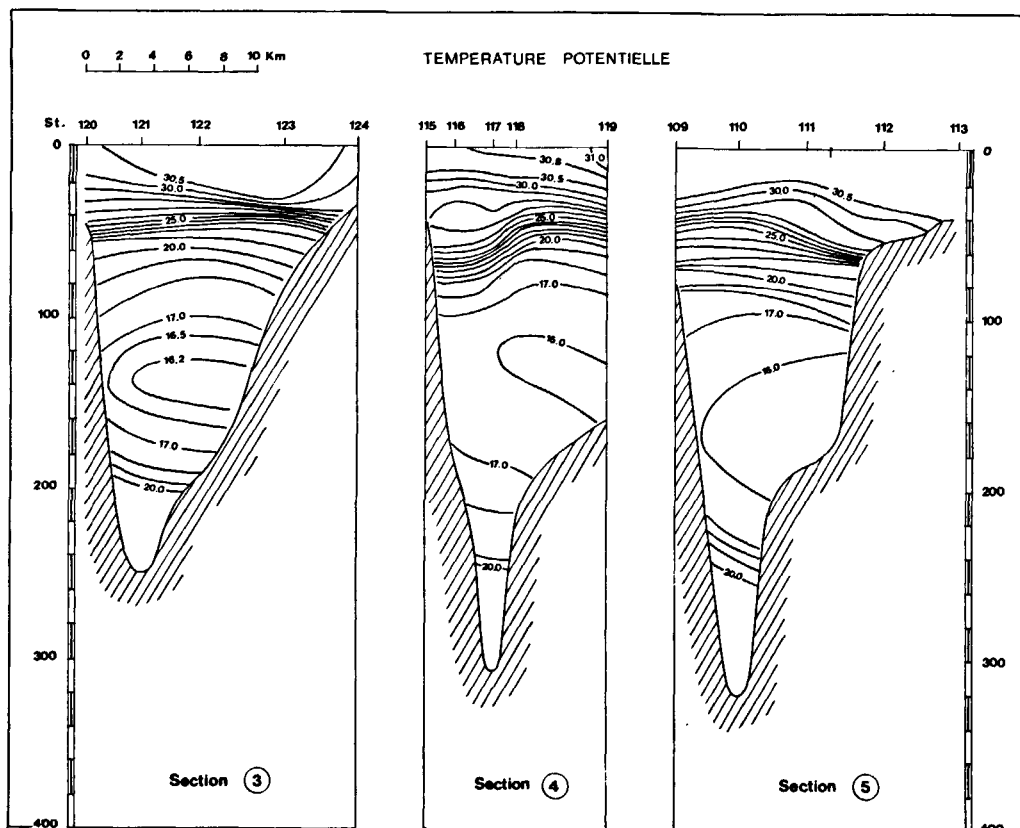


Figure 16  
 Vertical distribution of potential temperature in September along the transversal sections 3, 4 and 5.  
 Répartition verticale de température potentielle le long des sections transversales 3 à 5 du détroit de Bab el Mandeb en septembre.

Figure 17

Time variations (1 October at 12 h 25 to 2 October at 15 h 40) of the vertical distribution of temperature at two stations of the section 4:

Site A: 12°35.2'N-43°17.4'E;  
Site B: 12°37.4'N-43°20.4'E.

Variations temporelles du profil vertical de température entre le 1<sup>er</sup> octobre 12 h 25 et le 2 octobre 15 h 40 à deux stations de la section 4 :

point A : 12°35.2'N-43°17.4'E;  
point B : 12°37.4'N-43°20.4'E.

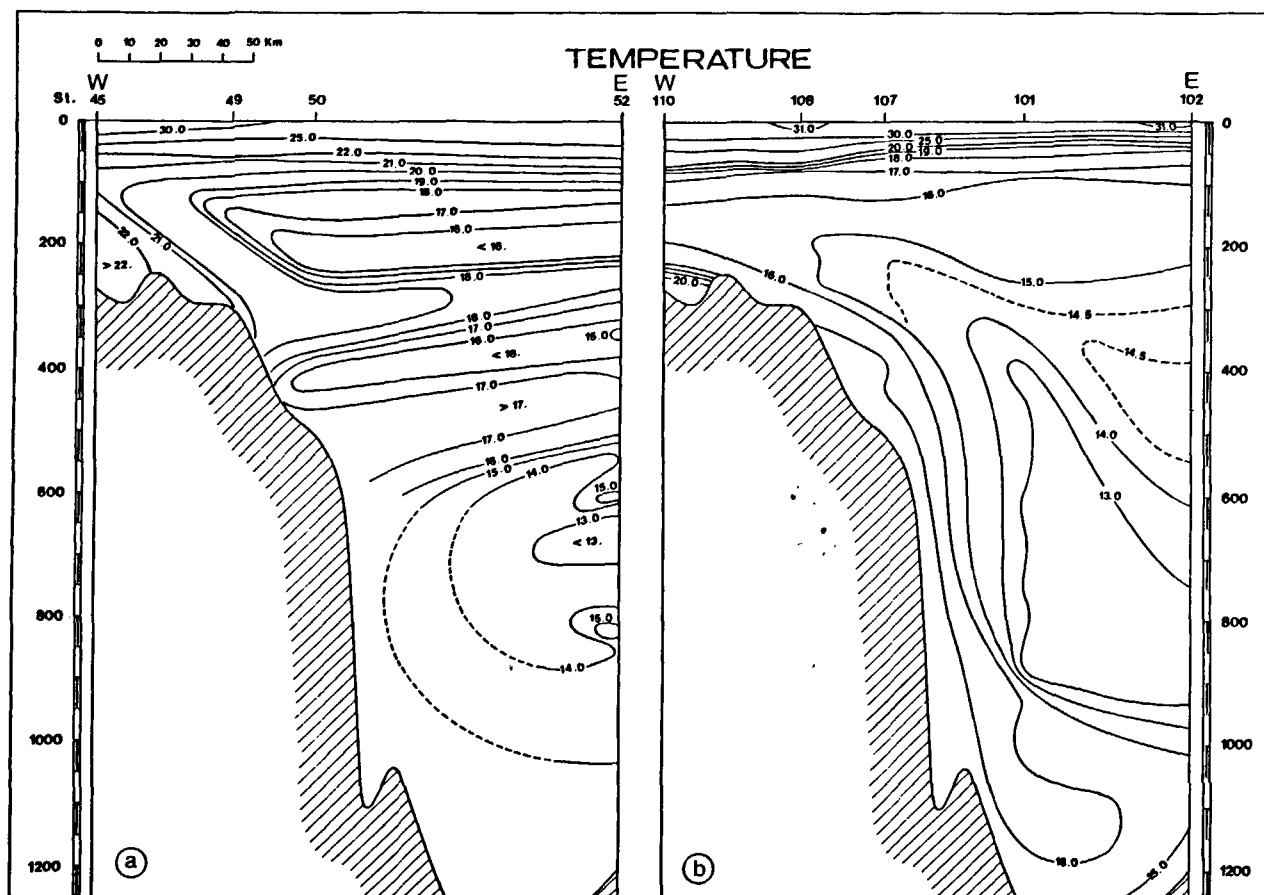
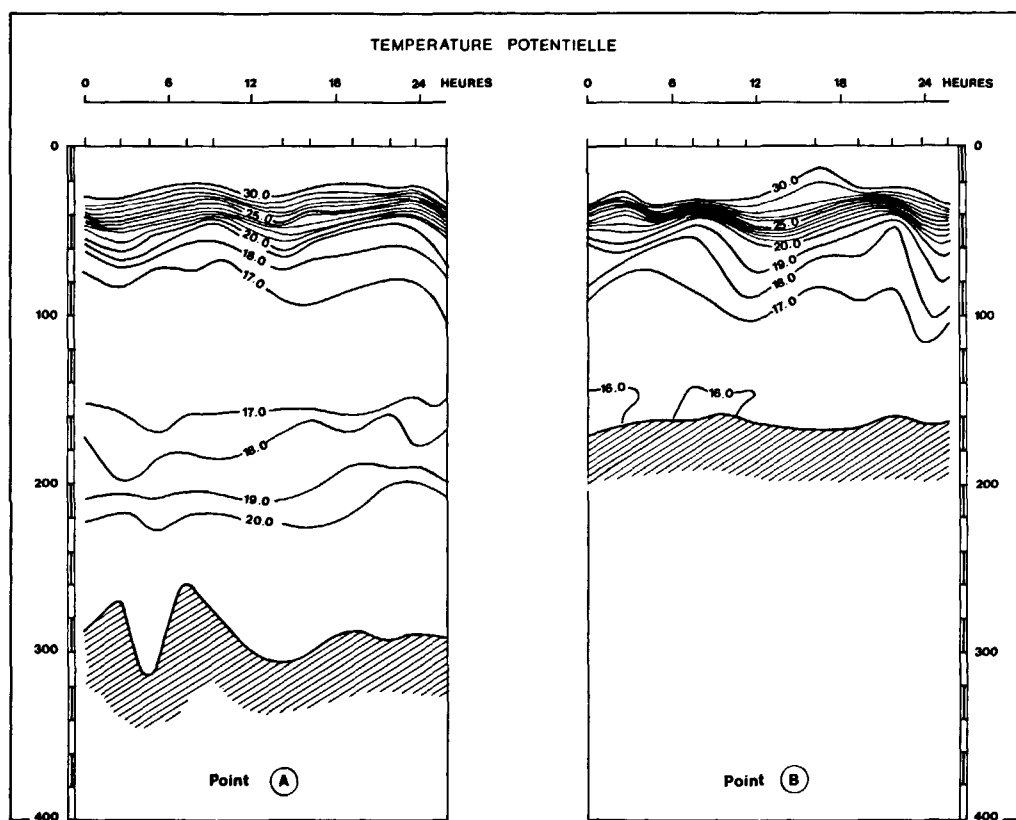


Figure 18

Vertical distribution of temperature in the deep fault of the Gulf of Aden:

a) in July;

b) in September.

Répartition verticale de température dans la fosse profonde du proche Golfe d'Aden :

a) en juillet;

b) en septembre.

Ocean. At the CTDO<sub>2</sub> stations made in the near Gulf of Aden (Fig. 2a), the Red Sea intermediate waters have the following characteristics:

The upper Red Sea layers have a typical thickness of about 100 dbar and are very variable with time. They are far more abundant and have higher temperatures at the beginning of summer (Fig. 18a) than at the end of the season (Fig. 18b). Thus the two upper Red Sea layers have respectively  $T \approx 19^\circ\text{C}$  near 300 dbar and  $T \approx 16.5^\circ\text{C}$  near 450 dbar in July (station 50 and 52). In September at the same location (station 107 and 102), the upper temperature maxima are less contrasted, colder by about  $3^\circ\text{C}$  and are found 100 dbar deeper. It must be noticed that the early summer temperature distribution does not represent the winter distribution. In January 1963 (Vangriesheim, 1974), the temperatures measured in the Red Sea intermediate waters were  $\theta \approx 20^\circ\text{C}$  at 300 dbar and  $\theta \approx 19^\circ\text{C}$  at 500 dbar. Very probably those layers are only fed during the winter season and the fast temperature decrease observed in summer must be due to the mixing with the relatively cold (about  $13^\circ\text{C}$ ) Indian Ocean surrounding water.

At the northern stations 52, 101, 102 where the depth exceeds 1000 dbar, a deep Red Sea water is found with  $\theta \approx 16^\circ\text{C}$ ,  $S \approx 37.5$ ,  $\text{O}_2 \approx 0.8$  ml/l,  $\sigma_\theta \approx 27.5$  in the core. This layer is thicker and more homogeneous than the upper Red Sea layers and spreads between 900 dbar and the bottom. There is no clear variation between July and September but unfortunately the station 101 site, where this water is the most abundant, was not investigated in July. In January 1963, the deep Red Sea layer seems to be attached to the nearest upper Red Sea layer, and warmer by  $1^\circ\text{C}$  than the summer 1982 value. This deep layer must come from the deepest part of the Red Sea overflow and, as it remains abundant in summer, some continuous feeding must exist.

## TIME VARIATIONS OF TEMPERATURE AND CURRENT IN THE BAB AL MANDAB STRAIT

We shall present first the results of the three summer months time series of temperature and velocity. Then an estimation of the depth of the interfaces between the different layers and an interpolation of the vertical velocity profile will be made in order to calculate the fluxes of water exchanged between the Red Sea and the Indian Ocean.

### Description of the observations

The mooring line was anchored at 189 m on the eastern side of the central trench in the Bab al Mandab Strait at the location  $12^\circ 35' \text{N}$ ,  $43^\circ 20' \text{E}$  (Fig. 2b). Two records lasted from 82/07/01 to 82/09/26 at 100 and 140 dbar and the upper currentmeter only from 82/07/06 to 82/07/18. Because of the strong currents existing in that region, the mooring line slanted many times and the pressure given by the pressure gauges at the average depth of 52 and 99 dbar were very variable. The

extreme values recorded are thus respectively 37 to 72 dbar and 91 to 121 dbar.

The current presents a strong tidal signal with a maxima of about  $1 \text{ m.s}^{-1}$  northwestwards, decreasing slightly between 52 to 140 dbar and giving a current reversal once a day. The tide is semi-diurnal with a diurnal inequality which appears in the rough data and in the spectra. The spectra have a minimum of energy in the period 2-3 days. In order to get the residual current and temperature, a low-pass Lanczos filter was used with a cut-off period (half power) of 2 days.

The residual current for the whole duration of the observations is northwestwards (Fig. 19), in agreement with the fact that the currentmeters are set in the cold Indian Ocean inflow. This fact is valid also for the beginning of the observations in July where the summer regime is not yet established. In July the current is strong at 52 and 100 dbar and weak at 140 up to 18 July where it increases suddenly to its mean value of about  $0.17 \text{ m.s}^{-1}$ . During the short period of 5 to 8 July, a bubble of intense northwestwards flow was measured at 140 dbar. Towards the end of the record, another energetic event of opposite direction appears from 6 to 9 September at 140 dbar; the velocity at 100 dbar then decreases and turns eastwards. This last event very likely indicates a transient increase of the deep water outflow. Beside those two events, some about 4 days fluctuations are detected on the residual current.

In order to have a quantitative set of values easy to handle, the residual current and temperature have been averaged on 10 days periods, except for the first period from 82/07/09 to 82/07/16, the length of which is imposed by the duration of the 52 dbar time series. The results are presented in Table 1.

The highest values of those 10 days averaged velocities appear during the period 82/07/25 to 82/08/04, with  $0.37 \text{ m.s}^{-1}$  at 100 dbar and  $0.23 \text{ m.s}^{-1}$  at 140 dbar. The lowest value of the 10 days average temperature is  $15.30^\circ\text{C}$  at 140 dbar at the end of August. Thus the maximum of current does not coincide at all with the core of minimum temperature (and salinity). At the last period, the magnitude of the current is reduced by a factor of about 2.

### Estimation of the summer interfaces

The depth of the interfaces can be determined with an acceptable accuracy during the hydrographic surveys; the middle of the thermoclines are then taken as the boundaries. The Perim cross-section (Fig. 2b) has been investigated three times respectively in July, in September and in October during the "tide section". For those three sections, the mean depth of the interfaces between the different water layers is given (Tab. 2). It must be noticed that the interfaces are not horizontal, but the equivalent levels which preserve the cross-sections of the layers have been computed.

The time variation of the interfaces between the hydrographic surveys have been inferred from the recorded temperatures at 100 and 140 dbar (Fig. 19). For this

Figure 19  
 a) July-September residual current in the intermediate Indian Ocean flow in the Bab al Mandab Strait;  
 b) Corresponding filtered temperature time series.

a) Courant résiduel dans la couche intermédiaire issue de l'Océan Indien au détroit de Bab el Mandeb de juillet à septembre;  
 b) Série correspondante de température.

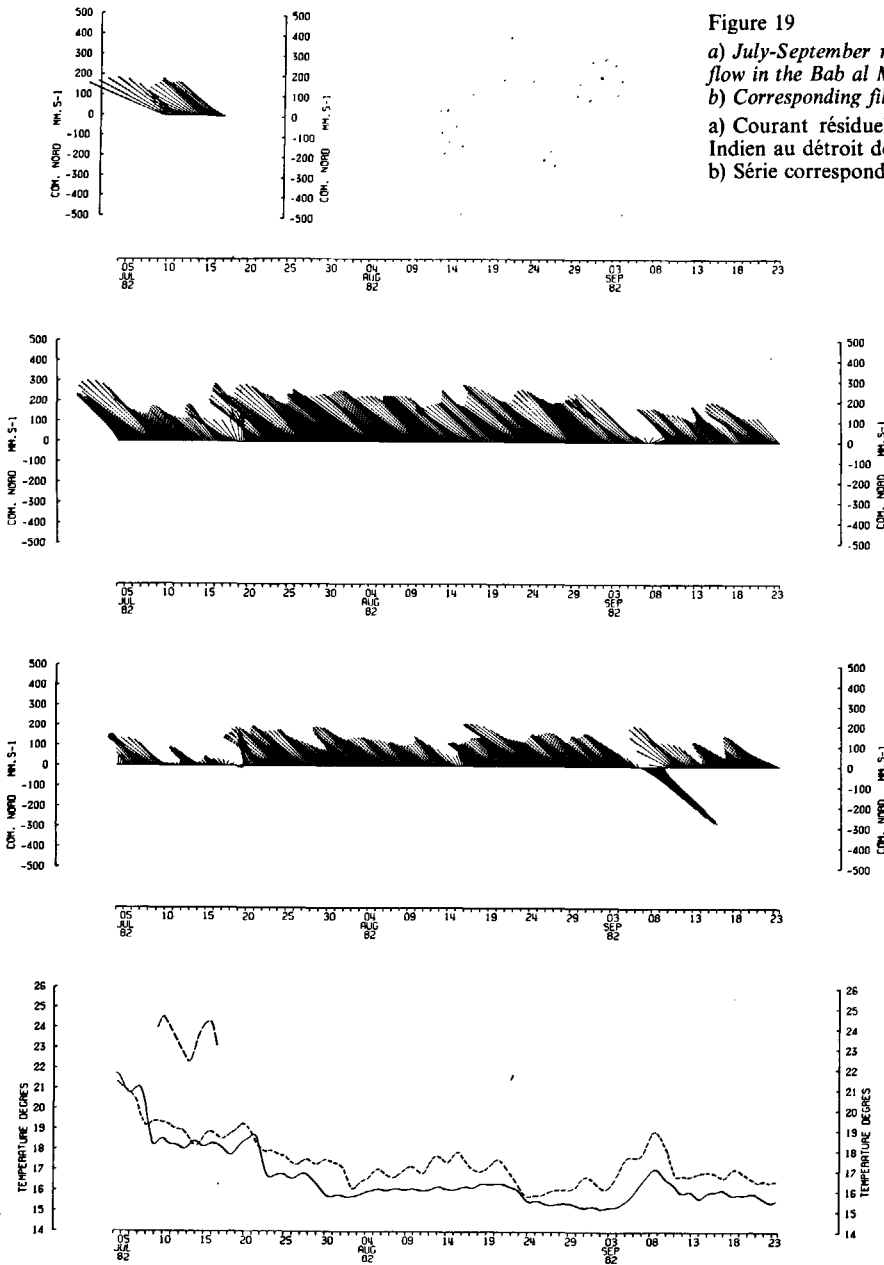


Table 1  
 10-day averages of current velocity ( $m.s^{-1}$ ) and temperature ( $^{\circ}C$ ).  
 Moyennes sur 10 jours de courant ( $m.s^{-1}$ ) et de température ( $^{\circ}C$ ).

Date	07/9-07/16	07/15	07/25	08/4	08/14	08/24	09/3	09/13	09/23
Pressure	52								
Speed	0.244								
Direction	304								
Temperature	23.66								
Pressure	100								
Speed	0.229	0.260	0.368	0.347	0.324	0.309	0.174	0.198	
Direction	314	315	309	311	310	314	316	314	
Temperature	18.79	18.39	17.03	17.07	16.93	16.13	17.55	16.72	
Pressure	140								
Speed	.069	0.132	0.232	0.185	0.201	0.219	0.043	0.126	
Direction	309	317	312	312	311	312	310	310	
Temperature	18.27	17.75	16.12	16.05	16.13	15.30	16.17	15.79	

Table 2

Data points used to determine the depth of the interfaces at the Perim cross-section at three different periods of time.

Données utilisées pour déterminer la profondeur des interfaces sur la section transversale de Périn à trois différentes époques.

Date	82/07/2	82/09/29	82/10/1-2
Upper interface T (°C)	27	25	25
Upper interface P (dbar)	36	52	40 ± 5
Lower interface T	22	19	19
Lower interface P	158	243	202 ± 8
Station	38 39	119 118	All 22 tide stations
T (100 dbar)	21.03	20.82	16.80 16.18 16.80 ± 0.34
T (140 dbar)	16.96	21.87	15.42 16.16 16.41 ± 0.22

we made the assumption that there is some relationship between the depth of an interface and the temperature at a fixed near point. The relationship has been sought on the temperature distributions of the three Perim cross-sections (see Fig. 20 and Tab. 2).

Among the simple functions (polynomial, hyperbola, exponential) which are exactly verified for these three data points, it is not possible to find any with no discontinuity, maximum or minimum inside the considered intervals of temperature and pressure. Thus we look for a least square regression with a function of the less order: A) a first degree polynomial; and B) a simple exponential in T. Those functions are given on Table 3 for both interfaces.

Table 3

Empirical functions relating the depth of the upper (lower) interface with the temperature at 100 (140) dbar interface.

Relations empiriques entre la profondeur de l'interface supérieure (inférieure) et la température à 100 (140) dbar.

	$P = A_0 T + A_1$	$P = B_0 \exp(B_1 T)$
Upper interface	$A_0 = -2.482$ $A_1 = 87.5$ St dev = 4.6	$B_0 = 121.17$ $B_1 = -0.05844$ St dev = 4.6
Lower interface	$A_0 = -14.028$ $A_1 = 449.4$ St dev = 13.3	$B_0 = 720.08$ $B_1 = -0.07293$ St dev = 12.7

The curves of the (B) exponentials (Fig. 20) have a curvature which fits better the observations than the (A) lines and it is noticeable that the coefficient which multiplies T in the (B) relations have the same order of magnitude for both interfaces. The exponentials (B) have then been chosen to calculate the depth Z1 and Z2 of the interfaces between the two legs of the cruise. The results for the 10-days average periods are given Figure 22a and Table 4. The upper interface does not change very much with time, but the lower interface sinks down to a maximum depth of about 240 dbar at the end of August in correlation with the minimum of temperature.

**Estimation of the current profiles and the fluxes**

With the depth of the boundaries (zero velocity) and the velocity at 100 and 140 dbar there are 4 data points

in each period except the first one where 5 points are available. Normally we ought to have used the baroclinic current resulting from the pressure horizontal gradient to complete the vertical current profile. Unfortunately this method did not work. The geostrophic component has been computed first between the stations 116 and 119 of the cross-section 4. Then the calculation has been made between the 11-stations ave-

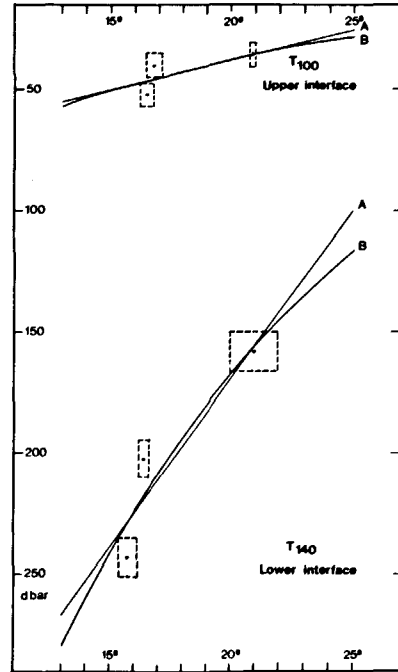


Figure 20  
Relationship between the depth of the interfaces and the temperature at a near fixed vertical level.  
Relation entre l'immersion des interfaces et la température aux points fixes les plus proches.

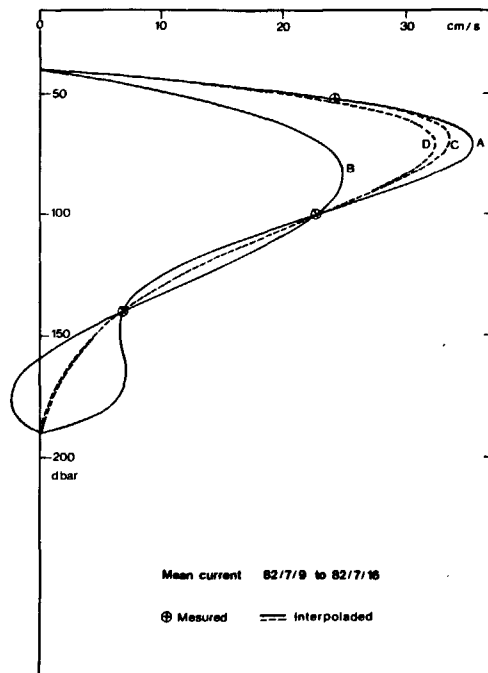


Figure 21  
Comparison between the results of several simple functions for interpolating the vertical velocity profiles for the period 9.07.82 to 16.07.82.  
Comparaison entre les résultats donnés par quelques fonctions simples pour interpoler le profil vertical de vitesse dans la période du 9.07 au 16.07.82.

Figure 22

a) Variation with time of the 10-day averaged velocity profiles computed with the method explained in text;  
 b) Corresponding flow of water.

a) Variation temporelle des profils verticaux de température en moyenne sur 10 jours et calculés par la méthode expliquée dans le texte;  
 b) Flux d'eau correspondants.

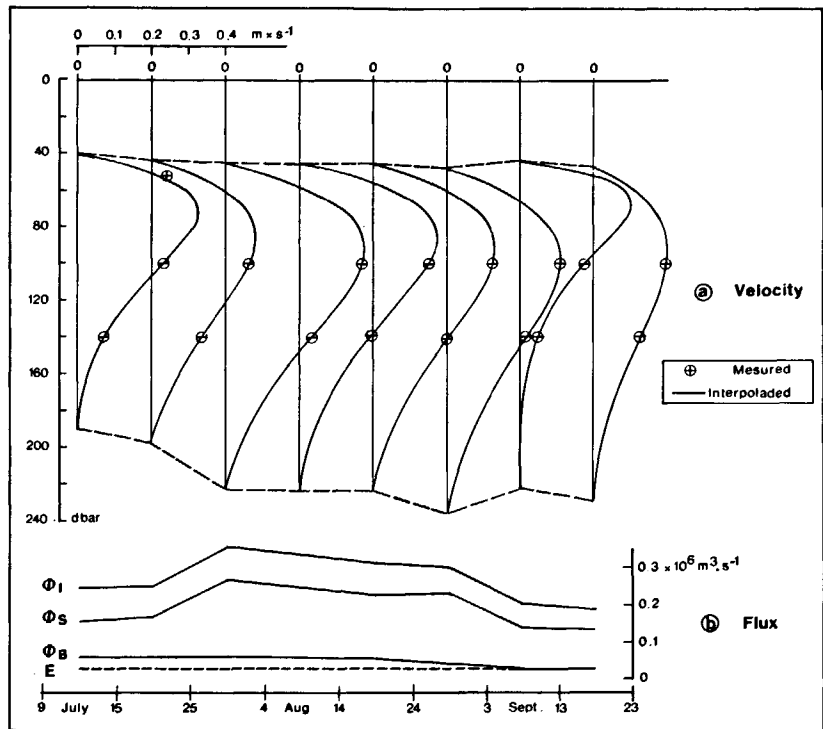


Table 4

10-day average fluxes ( $10^6 \text{ m}^3 \cdot \text{s}^{-1}$ ) during the summer 82.  
 Flux moyens sur 10 jours ( $10^6 \text{ m}^3 \cdot \text{s}^{-1}$ ) durant l'été 82.

Date	07/9-07/16	07/15	07/25	08/4	08/14	08/24	09/3	09/13	09/23
$\Phi_1$	0.25	0.25	0.36	0.34	0.32	0.31	0.21	0.19	
$\Phi_s$	0.16	0.17	0.27	0.25	0.23	0.24	0.14	0.14	
$\Phi_B$	0.06	0.06	0.06	0.06	0.05	0.04	0.03	0.03	
$Z_1$	40	41	45	45	45	47	43	46	
$Z_2$	190	197	222	223	222	236	221	228	

rage profiles of dynamic height at the tide stations A and B. In both cases, the current variation between the surface and 160 dbar remained within  $0.02 \text{ m} \cdot \text{s}^{-1}$  with a small maximum near 60 dbar. This does not fit the direct current measurements. There are many reasons which can explain the fact: the current is not geostrophic in the upper layer, the section has been made a few days after the currentmeter recovery and the currents are slowing down very fast in this transition period. Thus another method has to be used.

As previously a simple function of the pressure has been sought for interpolating the velocity and tested upon the 9 to 16 July period where there are 5 data points on the vertical. There is no polynomial which, at the same time fit the 5 data points (or 4 points if we exclude the 52 dbar level) and have only one maximum inside the 40-200 dbar layer (see Fig. 21, curves A and B). The exponential fits give better results (Fig. 21, curves C and D) and then their calculation is given below.

The 5 data points curve C represents the function:

$$V = V_0 \sin \pi \frac{Z - Z_1}{Z_2 - Z_1} \exp A (Z - Z_0)^2$$

$Z_1, Z_2$ : pressure of the boundaries

$V_0, A, Z_0$ : constants determined by the three records

and the 4 data points curve D, the function:

$$V = V_0 \sin \pi \frac{Z - Z_1}{Z_2 - Z_1} \exp(AZ) \quad A < 0.$$

Both profiles are very close to each other and the second one, which is simpler and can be deduced later from the two lowest time series, will be used to estimate the current vertical profiles. The profiles thus computed are given in Figure 22a. The velocity maxima appear near 90 dbar, but at the beginning and the end of the record, this velocity maximum is met about 20 dbar above that level.

The intermediate fluxes ( $\Phi_1$ ) are computed by integration of the velocity profiles over the whole thickness of the intermediate layer with a step of 5 dbar. An order of magnitude of the opposite fluxes in the surface layer ( $\Phi_s$ ) and in the bottom layer ( $\Phi_B$ ) is found from the conservation of mass equation:

$$\Phi_1 = \Phi_s + \Phi_B + E$$

$$E = \text{evaporation} = 0.03 \times 10^6 \text{ m}^3 \cdot \text{s}^{-1}$$

and from the assumption that the Red Sea fluxes are proportional to the surfaces S through which they flow:

$$\Phi_s / \Phi_B = S_s / S_B.$$

The corresponding values are given Table 4 and Figure 22b together with the depth of the interfaces (in dbar).

The largest surface and intermediate fluxes are found during the period 82/07/25 to 82/08/04 when the currentmeters recorded the fastest residual current. Afterwards the two upper fluxes decrease to about half the maximum value at the end of September. The deep Red Sea outflow appears simply to decrease from the beginning to the end of the observations; in September the flux has an estimated value which is about the same that the evaporation over the Red Sea.

## DISCUSSION AND SUMMARY

The summer regime is marked by the sinking of the Indian Ocean inflow at an intermediate level. At the beginning of July, the head of this cold, fresh and poorly oxygenated water has not yet reached the sill location and the Red Sea regime keeps a winter pattern. In October, the intermediate Indian Ocean flow reaches its northernmost position near 18°N in the Red Sea. There some meandering is observed. Neglecting the mixing, the distance covered by the head front of the intermediate flow between the two legs of the cruise is about 450 km in 100 days, which means an average velocity of 0.05 m.s<sup>-1</sup>. The current velocities recorded in the Bab al Mandab Strait are higher by a factor of 3 to 5. The widening of the Red Sea north of the sill is very likely the source of eddy formation and slowing-down of the flow.

A southward increase of temperature and decrease of density appears clearly in the Red Sea deep water below 800 dbar. This horizontal gradient in the deep layer seems to be a summer feature due to a faster mixing with the overlying water. Yet the study of the seasonal variations in the deep Red Sea water needs more observations than the present data set. The only certain fact is that the sinking of the surface water in the northern Red Sea cannot reach the very deep layer, but only a subsurface level, because the temperatures are too high. The direct current measurements made during the Marion Dufresne cruise have very much increased the very sparse set of available data. They have allowed an estimation of the summer inflow flux, and its evolution with time. Thus the boundary between the surface Red Sea outflow and the intermediate Indian Ocean flow appears to stay at 42 ± 5 dbar during all the summer. The lower boundary between the intermediate flow and the deep Red Sea outflow sinks from about 160 dbar in the beginning of July to about 240 dbar in September. The flow is the most intense upon the 07/25 to 08/04 period with an estimated inflow of 0.36 × 10<sup>6</sup> m<sup>3</sup>.s<sup>-1</sup>. This maximum summer value amounts to 65% of the maximum winter inflow estimated in December by Siedler (1968). The average summer

inflow on the whole period of observation is 0.28 × 10<sup>6</sup> m<sup>3</sup>.s<sup>-1</sup>. If we subtract the flux of evaporated water (0.03 × 10<sup>6</sup> m<sup>3</sup>.s<sup>-1</sup>) we get the value of the average total Red Sea outflowing flux in summer, which is 76% of the annual mean value of the outflow (0.33 × 10<sup>6</sup> m<sup>3</sup>.s<sup>-1</sup>, according to Siedler, 1969). Thus in summer there is a slow-down of about 30% in the exchanges between the Red Sea and the Indian Ocean.

The summer outflow splits with two layers. Most of the flux is concentrated in the surface layer with a maximum of 0.27 × 10<sup>6</sup> m<sup>3</sup>.s<sup>-1</sup> in the 07/25 to 08/04 period too. This value is slightly above the August value of 0.21 × 10<sup>6</sup> m<sup>3</sup>.s<sup>-1</sup> estimated by Patzert from the ship drifts. The error on such an estimation is large and the measurements presented here have a better accuracy. Yet it appears that the magnitudes of both determinations are the same.

During this experiment, the deep Red Sea outflow appeared very weak, and of the same order of magnitude as the evaporated flux at the end of summer. It would appear that just before the autumn reversal of the currents, the deep Red Sea overflow is practically stopped. The presently estimated values amount to 12% of the winter overflow in early summer and only 6% at the end. The cooling and vanishing of the upper intermediate (above 1000 dbar) warm Red Sea layers in the near Gulf of Aden during the summer season is a direct effect of the vanishing of the source. Yet the lowest (1200 dbar) and less warm Red Sea water of the Gulf of Aden is always found at the end of summer and probably receives the reduced volume of the deep overflow.

## Acknowledgements

This work has been carried out with the support of T.A.A.F., CNEXO and UNESCO. The authors are grateful to the crew of the "Marion Dufresne" and their colleagues of the Centre de Brest, of the Museum d'Histoire Naturelle de Paris and the Laboratoire de Physique et Chimie Marines de l'Université de Paris VI who participated in the experiment and who helped in the preparation of this paper. The currentmeter moorings were prepared and laid out by R. Perchoc and G. Hesloin, and the CTD data were collected with A. Kartavtseff, C. Levy (1st leg) and J.-P. Gouillou, A. Billant, R. Joly (2nd leg). The computer programmes for the CTD data processing were written by N. Le Guen, M. Le Breton and J.-P. Beucher. The currentmeter data were processed with the Woods Hole Oceanographic Institution routine. The drawings were made by J. Kervella and the typing by J. Le Gall. We also thank Y. Desaubies for corrections and constructive remarks on the text and M. Marchalot for correcting the final version.

## REFERENCES

- Baudner H., Jancke K., Quadfasel D.**, 1984. CTD-data obtained in the Red Sea during 21-30 May 1983, R/V Sagar Kanya, Institut für Meereskunde der Universität Hamburg, Tech. Rep., 1-84, 71 p.
- Bibik V. A.**, 1968. Peculiarities of the hydrological conditions in the northern part of the Red Sea in the winter season of 1964-1965, *Okeanol. Issl.*, **19**, 201-213.
- Hassan E. M., Soliman G. H.**, 1985. Hydrography of the northern Red Sea (in prep.).
- Jones E. N., Browning D. G.**, 1971. Cold water layer in the southern Red Sea, *Limnol. Oceanogr.*, **16**, 3, 503-509.
- Koninklijk Nederlands Meteorologisch Instituut**, 1949. Red Sea and Gulf of Aden oceanographic and meteorological data, **129**, 26 p.
- Maillard C.**, 1971. Étude hydrologique et dynamique de la Mer Rouge en hiver, *Ann. Inst. Oceanogr.*, **498**, 2, 113-140.
- Maillard C.**, 1974. Eaux intermédiaires et formation d'eau profonde en Mer Rouge, in : *L'océanographie physique de la Mer Rouge*, Paris, 1972, 105-133.
- Maillard C., Soliman G. F.**, 1985. Mesures de physique effectuées en Mer Rouge à bord du N.O. « Marion Dufresne » en été 1982, *Rapp. Sci. Tech. TAAF*, n° 82.06, 173 p.
- Morcos S. A.**, 1970. Physical and chemical oceanography of the Red Sea, *Oceanogr. Mar. Biol. Ann. Rev.*, **8**, 73-202.
- Morcos S. A., Soliman G. F.**, 1974. Circulation and deep water formation in the northern Red Sea in winter, in : *L'océanographie physique de la Mer Rouge*, Paris, 1972, 91-103.
- Neuman C., Mc Gill D.**, 1961. Circulation of the Red Sea in early summer, *Deep-Sea Res.*, **8**, 223-235.
- Patzert W. C.**, 1972. Seasonal variations in structure and circulation in the Red Sea, *Ph. D. Thesis Dissert., Univ. Hawaii*, 103 p.
- Phillips O. M.**, 1966. On turbulent convection currents and the circulation of the Red Sea, *Deep-Sea Res.*, **13**, 6, 1149-1160.
- Robinson M. K.**, 1973. Monthly mean surface and subsurface temperature and depth of the top of the thermocline, Red Sea, Fleet numerical Weather Central, Monterey, Tech. note 73-4, 117 p.
- Siedler G.**, 1968. Schichtungs- und Bewegungsverhältnisse am Südausgang des Roten Meeres, "Meteor" *Forschungsergebn.*, **A**, **4**, 1-76.
- Siedler G.**, 1969. General circulation of water masses in the Red Sea, in: *Hot brines and recent heavy metal deposits in the Red Sea*, edited by E. T. Degens and D. A. Ross, Springer, New York, 131-137.
- Soliman G. F.**, 1979. Application of the hydrodynamical equations to the circulation in the Red Sea, *Ph. D. Thesis Dissert., Cairo Univ.*, 90 p.
- Van Akken H. M., Otto L.**, 1974. Observation of the exchange of water in the straits Bab al Mandab, in: *L'océanographie physique de la Mer Rouge*, Paris, 1972, 229-252.
- Vangriesheim A.**, 1974. Structure hydrologique et dynamique du Golfe d'Aden d'après la V<sup>e</sup> campagne du « Robert Giraud », *Rapp. Int. Mus. Hist. Nat.*, Paris, 31 p.
- Vercelli F.**, 1927. Campagne Idrografica della R.N. Amrairaglio Magnaghi in Mar Rosso 1923-1924, *Ann. Idrogr.*, **2**, 1-208 and 267-290.
- Werner F., Lange K.**, 1975. A bathymetric survey of the sill area between the Red Sea and the Gulf of Aden, *Geol. Jahrb.*, **D 13**, 125-130.
- Wyrski K.**, 1974. On the deep circulation of the Red Sea, in: *L'océanographie physique de la Mer Rouge*, Paris, 1972, 135-163.